THE ASTROPHYSICAL JOURNAL, 320:182–198, 1987 September 1

H I SUPERCLOUDS IN THE INNER GALAXY

BRUCE G. ELMEGREEN
IBM Watson Research Center; and Institute for Theoretical Physics

AND

DEBRA MELOY ELMEGREEN
IBM Watson Research Center; Institute for Theoretical Physics; and Vassar College Observatory
Received 1986 October 20; accepted 1987 February 13

ABSTRACT

Atomic hydrogen clouds in the Weaver-Williams 21 cm survey are found in the vicinity of the largest molecular cloud complexes in the first Galactic quadrant. The atomic masses are estimated in several ways, including a new method where the clouds are assumed to be composed of cool clumps immersed in a warm interclump medium. The clouds are found to contain between 10^6 and 4×10^7 $M_\odot$ of atoms at an average density of ~ 9 cm^{-3}. They appear gravitationally bound, their molecular mass fractions decrease from 70% to 5% with increasing distance from the Galactic center, and they are located in the spiral arms. The importance of these clouds for the large-scale distributions of interstellar mass, molecular fraction, and star formation is discussed.

Subject headings: interstellar: matter — interstellar: molecules — radio sources: 21 cm radiation

I. INTRODUCTION

An association between atomic hydrogen and carbon monoxide is present on scales ranging from small dark clouds to giant cloud complexes. This paper is concerned with the largest complexes, which have total masses in excess of $\sim 10^6$ $M_\odot$. H I clouds in the vicinity of giant CO clouds cataloged by Dame *et al.* (1986) and Myers *et al.* (1986) are identified from (l, v) and (l, b) maps of the Weaver and Williams (1973) 21 cm survey. The atomic masses and molecular fractions of these clouds are estimated, and the degree of self-gravitational binding is assessed.

Other observations of H I associated with CO are usually on a smaller scale. Surveys at 21 cm (Cleary, Heiles, and Haslam 1979) reveal relatively small atomic envelopes around most of the local molecular clouds (Sandqvist, Lindblad, and Lindroos 1976; Elmegreen 1985). Detailed maps show H I directly associated with molecular clouds in many sources, including Per OB2 (Sancisi *et al.* 1974), Sco OB2 (Strauss, Pöppel, and Vieira 1979), Ceph OB3 (Dewdney 1982), M17 (Sato and Fukui 1978), W3/W4 (Read 1981*a*; Hasagawa, Sato, and Fukui 1983), W33 (Sato 1977), W41 (Gordon, Gordon, and Jacobsen 1976), W58 (Read 1981*b*), ρ Oph (Myers *et al.* 1978; Minn 1981), Taurus (Wilson and Minn 1977; Batrla, Wilson, and Rahe 1981; Pöppel, Rohlfs, and Celnik 1983), NGC 1579 (Dewdney and Roger 1982), NGC 5146 (Roger and Irwin 1982), NGC 7538 (Read 1980; Dickel, Dickel, and Wilson 1982), L134 (Winnberg *et al.* 1980), L1778/L1780 (Mattila and Sandell 1979), Khavtasi 141 (Saito, Ohtani, and Tomita 1981), and an OB association near GY Sge (Bania 1983). H I self-absorption is also observed in nearby dark clouds (Bok, Lawrence, and Menon 1955; Knapp 1974 and references therein; Chu 1975). The atomic masses of these regions are usually 10^3–10^5 $M_\odot$, less in the case of the small dark clouds. These masses are much smaller than the H I cloud masses derived here.

The large-scale association between H I and CO is of interest for studies of cloud and star formation in galaxies. The presence of such an association was previously recognized from general surveys (Burton, Listz, and Baker 1978; Baker and Burton 1979; Liszt, Burton, and Bania 1981; Peters and Bash 1982; Dame 1983), although individual H I clouds were not studied in detail. The only $\sim 10^7$ $M_\odot$ cloud previously identified in the inner galaxy is the obvious one surrounding M16 and M17 (at [l, v] = [12, 14] in the present survey). This cloud was already mapped (Elmegreen 1979) from the Weaver and Williams (1973) survey and compared to CO from the survey by Cohen, Dame, and Thaddeus (1986). The extensive scale for star formation in this region was also discussed by Stal'bovskii and Shevchenko (1981). The lack of recognition of $\sim 10^7$ $M_\odot$ clouds in the inner Galaxy contrasts sharply with the ease of detecting such clouds in the outer Galaxy (McGee and Milton 1964; Henderson, Jackson, and Kerr 1982), presumably because there is no kinematic distance ambiguity in the outer Galaxy, and because most of the gas there is atomic. The outer Galaxy H I clouds have also been found to be associated with CO (Grabelsky *et al.* 1987), although the molecular fraction there is much less than it is for giant clouds in the inner Galaxy (§ IV).

Atomic clouds similar to those studied here are also evident in aperture synthesis maps of H I in other spiral galaxies, such as M33 (Wright, Warner, and Baldwin 1972; Newton 1980*a*), M101 (Allen, Goss, and van Woerden 1973; Allen and Goss 1979; Viallefond, Allen, and Goss 1981; Viallefond, Goss, and Allen 1982), M81 (Rots 1975), M31 (Emerson 1974; Unwin 1980*a*, *b*; Bajaja and Shane 1982), M106 (van Albada 1980) and IC 342 (Newton 1980*b*). A compilation of the properties of such clouds, and a demonstration that they could be gravitationally bound against galactic tidal forces, was made previously (Elmegreen 1987*a*). Clouds of this mass are also present in Magellanic-type irregular galaxies, including the LMC (McGee and Milton 1966; Page and Carruthers 1981), IC 2574 (Seilestad and Wright 1973), Ho II (Cottrell 1976), and NGC 6822 (Gottesman and Weliachew 1977). Molecular emission from the vicinity of giant H I clouds has been observed in the galaxies M101 (Blitz *et al.* 1981; Blitz 1985), M31 (Boulanger, Stark, and Combes 1981; Boulanger *et al.* 1984; Linke 1982; Stark 1985; Nakano *et al.* 1986) and M51 (Rydbeck *et al.* 1986).

The purpose of the present paper is to identify and study the most prominent H I emission features in the first Galactic quadrant. The identifications are made in § II, the cloud masses are derived in § III, and the correlation between H I and CO is discussed in § IV. The possibility that some of the H I emission features are not distinct clouds but only intensity maxima created by velocity crowding is discussed in § V. Virial-theorem velocity dispersions are then calculated in § VI for the clouds most likely to be unblended, and they are compared to the observed H I line widths to assess the state of self-gravitational binding. The observed densities are also compared to the critical densities for tidal binding. A discussion of the importance of these clouds for the mass and energy content of the interstellar medium and for star formation is in § VII.

II. IDENTIFICATION OF THE H I FEATURES

A longitude-velocity diagram of the H I emission from the first Galactic quadrant was made from the computer tape version of the Berkeley low-latitude H I survey (Weaver and Williams 1973). The observed temperatures were clipped at 40 K to emphasize the bright cloudy structure, and each temperature was multiplied by the near kinematic distance, $D(l, v)$, before plotting (for reasons discussed below). Figure 1*a* shows a contour plot and Figures 1*b* (Plate 3) and 1*c* (Plate 4) show gray scale plots of this distance-normalized, temperature-clipped longitude-velocity diagram. The plotted quantity is

$$I(l, v) = \frac{D(l, v)}{20°} \int_{-10°}^{10°} T_{40}(l, b, v) db, \quad (1)$$

where, for H I antenna temperature, T_A,

$$T_{40}(l, b, v) = T_A(l, b, v) \quad \text{if} \quad T_A(l, b, v) > 40 \text{ K}$$

and (2)

$$T_{40}(l, b, v) = 0 \quad \text{if} \quad T_A(l, b, v) < 40 \text{ K} .$$

A value of 40 K was chosen for clipping because this corresponds to the expected antenna temperature for a "standard" diffuse cloud (Spitzer 1978), and because the large emission regions studied here appear to be well separated by 40 K minimum contours. Approximately 60% of the total 21 cm line luminosity from the first quadrant was found to be from emission at $T_A > 40$ K.

Contour values in Figure 1*a* start at 0 K kpc and increase in increments of 5 K kpc. The quantity plotted in Figure 1*b* is a

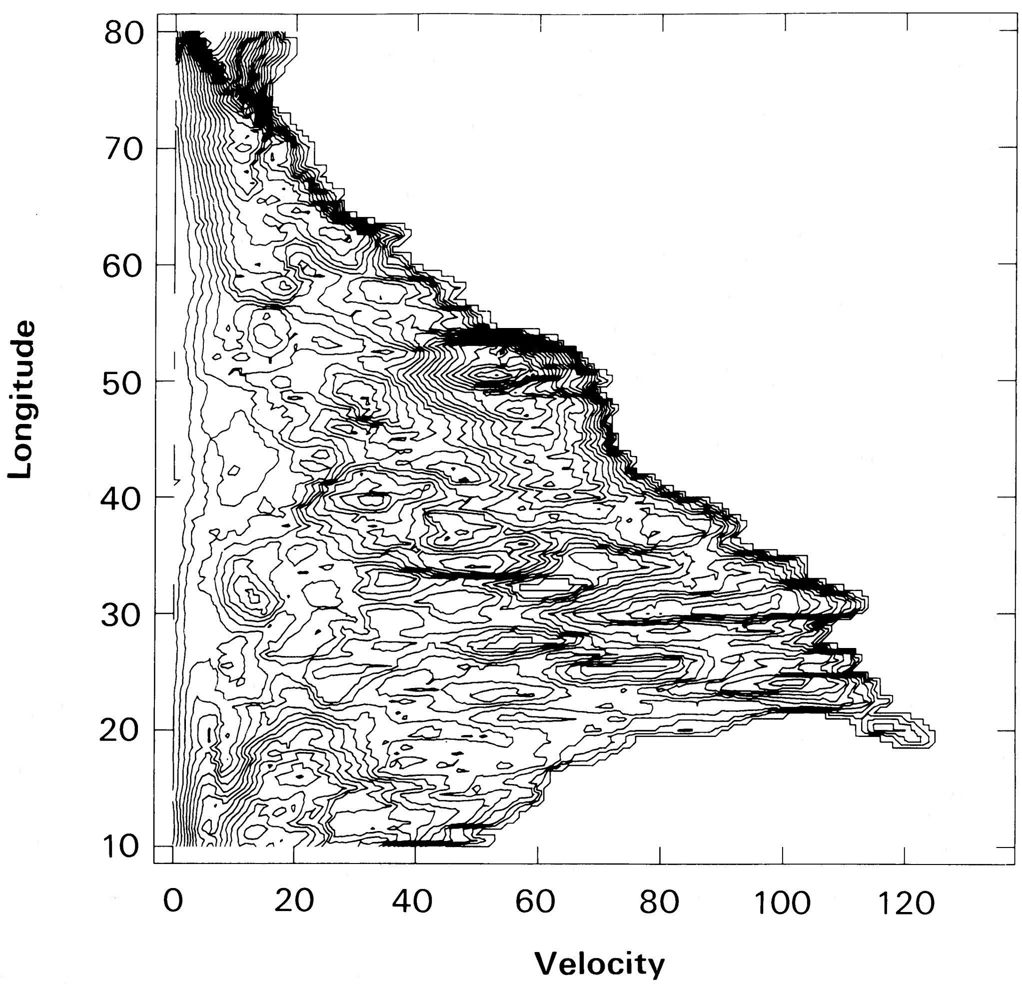

FIG. 1*a*.—Contour map of 21 cm emission from the first quadrant, clipped at 40 K antenna temperature and multiplied by the near-kinematic distance; from the Weaver and Williams (1973) survey. Contour values start at 5 K kpc and increase in increments of 0 K kpc. Velocity is in km s^{-1} and Galactic longitude is in degrees.

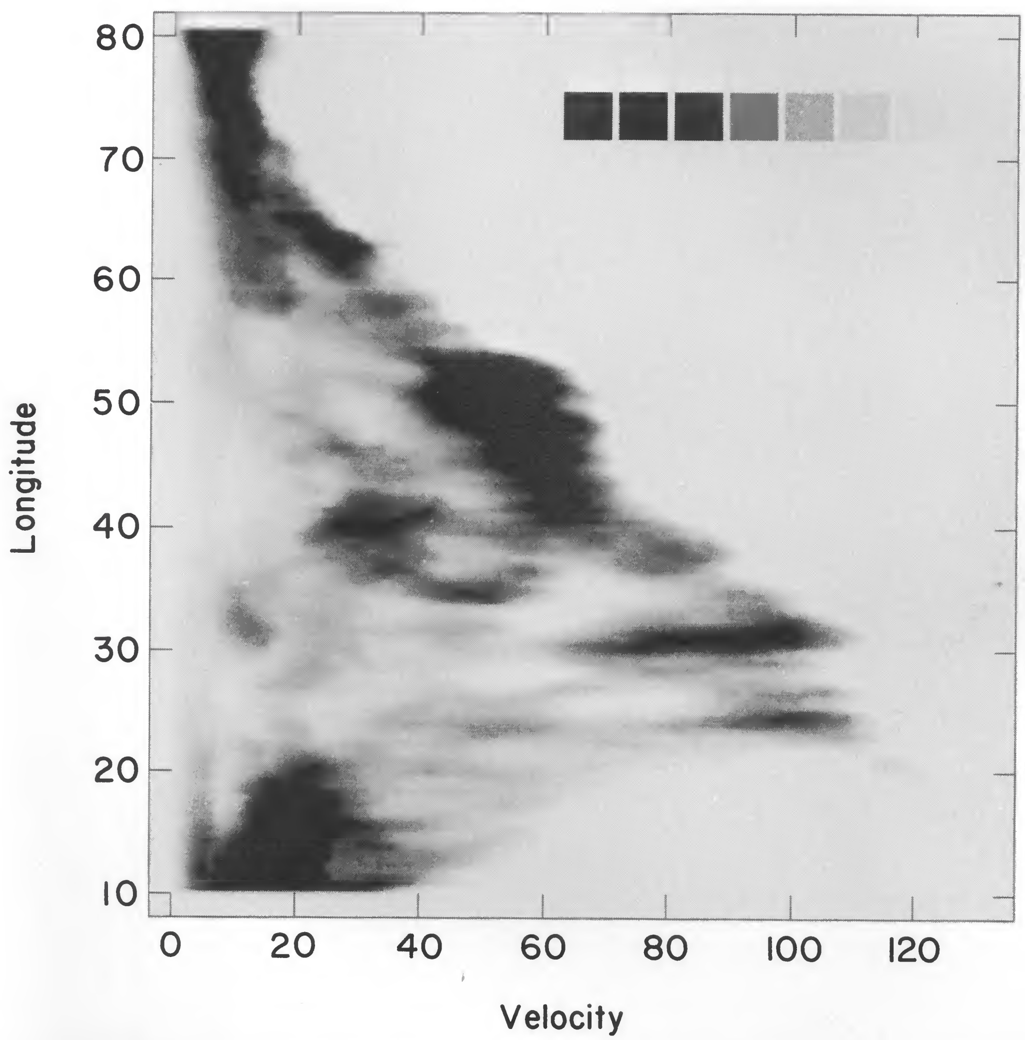

FIG. 1*b*.—Gray scale representation of Fig. 1*a*. Gray scale boxes start at 10 K kpc for the lightest shade, and increase in increments of 10 K kpc up to 70 K kpc for the darkest shade.

ELMEGREEN AND ELMEGREEN (*see* **320**, 183)

1987ApJ...320..182E

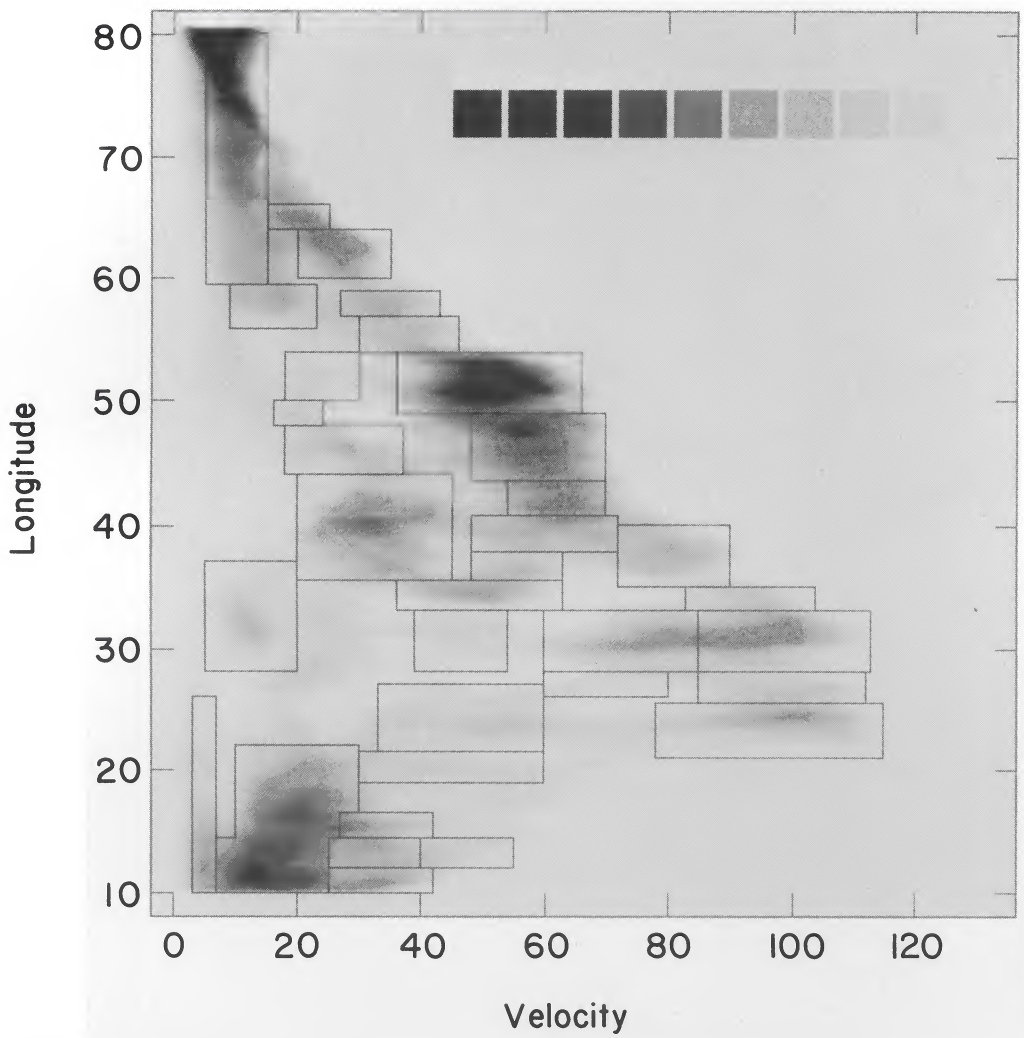

FIG. 1c.—Gray scale representation of Fig. 1a, with boxes outlining the H I clouds defined in Table 1. Gray scale boxes start at 20 K kpc for the lightest shade and increase in increments of 10 K kpc up to 100 K kpc for the darkest shade.

ELMEGREEN AND ELMEGREEN (*see* **320**, 183)

gray scale representation of Figure 1*a*. The scaling boxes start at 10 K kpc for the lightest and increase in increments of 10 K kpc up to 70 K kpc for the darkest. The rectangles in Figure 1*c* outline the positions of the giant H I clouds discussed here. The gray scale boxes in Figure 1*c* start at 20 K kpc and increase up to 100 K kpc in steps of 10 K kpc. Figures 1*b* and 1*c* have different gray levels so that a wide total range of emission brightnesses can be distinguished.

The kinematic distance, $D(l, v)$, has been included in the definition of $I(l, v)$ so that similar contour values at different (l, v) represent the same projected H I mass density. The distance converts the angular coordinate db into a linear scale. Without D, the emission from a cloud at a large distance would appear less prominent on an *l-v* diagram than the emission from a similar cloud at a small distance. The *near-kinematic* distance was chosen for all of the emission in Figure 1 because many of the prominent clouds can be associated with one or more near-distance CO clouds in the survey by Dame *et al.* (1986), as discussed in § IV. The clouds at the far distance on the (l, v) diagram will appear relatively weak after this distance multiplication, but they are still apparent, as discussed below. The distance multiplication and temperature clipping highlights the emission features. The near distance alone does this well enough because the near distance has a much larger dynamic range than the far distance; the near distance spans approximately a factor of 10, from ~ 1 kpc to ~ 10 kpc, so most of the dilution of the projected column density on a conventional (l, v) diagram can be removed if each temperature is multiplied by the near kinematic distance. The far distance spans only a factor of 2, from ~ 10 kpc to ~ 20 kpc, so only a little definition is lost by using the near distance exclusively, instead of the true distance. (Of course, the derivation of cloud masses in § III will use the true distance.)

Figures 2*a*, 2*b*, and 2*c* (Plates 5, 6, and 7) display spatial (l, b) maps of the antenna temperature in single velocity channels (of width 2.11 km s^{-1}) for velocities between 10 and 100 km s^{-1}, in steps of 10 km s^{-1}. The gray scale calibration boxes start at 20 K for the lightest shade, and increase in increments of 10 K up to 100 K for the darkest shade. Bracketed lines in each plot indicate the longitude ranges covered by the rectangles in Figure 1*c*.

The coordinates of the prominent H I features in Figures 1 and 2 are summarized in Table 1. The first column gives an identifying coordinate of the emission peak in each of the rectangles in Figure 1*c*, and the next three columns give the range of coordinates covered by the rectangles, or by the latitude extents, as shown in Figures 1*c* and 2. The distance, D, comes from the appropriate near or far kinematic distance, or from the distance to associated CO clouds as discussed in § IV. The Sun's distance to the Galactic center was assumed to be 10 kpc.

Some of the H I cloud boundaries and divisions between clouds are arbitrary because the associated emission regions are not distinct. This makes some of the cloud masses, radii, and velocity dispersions highly uncertain. The total mass of all the clouds should be more reliable, because the mass that was not counted for one cloud is likely to be counted for another.

Other identification errors may be caused by opacity variations, which can produce artificial boundaries or give single clouds the appearance of two clouds separated by emission minima. Such errors are not likely to be frequent because maps of H I self-absorption (references in § I) usually show only small regions (<10 pc), which do not produce noticeable

TABLE 1

H I CLOUD IDENTIFICATIONS

(l, v) (°, km s^{-1})	Δl	Δb	Δv (km s^{-1})	D (kpc)
10.5, 33	10°–12°	−2° to 1°	25–42	4.7
12, 6	10 –26	−10 to 10	3–7	0.3
12, 14	10 –22	−4 to 6	7–30	2.2
13.5, 32	12–14.5	−1 to 2	25–40	4.4
13.5, 47	12–14.5	−1 to 2	40–55	5.4
15, 28	14.5–16.5	−3 to 3	27–42	4.4
19.5, 42N/F	19–21.5	−2 to 2	30–60	4.2/14
23, 54N/F	21.5 –27	−2 to 2	33–60	4.1/14
24, 102N/F	21 –25.5	−1 to 1	78–115	7.1/12.6
26, 105	25.5 –28	0 to 1	85–112	9
27, 64	26 –28	−1 to 1	60–80	4.9
30, 78	28 –33	−2 to 1	60–85	5.7
30.5, 94	28 –33	−1 to 1	85–113	6.9
31, 47N/F	28–33	−1 to 2	39–54	3.3[a]/14
31.5, 13N/F	28 –37	−10 to 7	5–20	0.9/16
34, 50	33–35.5	−2 to 3	36–63	3.1
34, 95	33 –35	0 to 1	83–104	8.3
36, 58	35.5 –37.7	−1 to 2	48–63	12
37.5, 81	35 –40	−1 to 2	72–90	9.5
39.5, 33	35.5–44	−5 to 7	20–45	2.5
40, 64	37.7 –40.7	−2 to 3	48–72	11
41, 62	40.7 –43.5	−2 to 1	54–70	10
46, 28	44 –48	−4 to 7	18–37	1.8
47.5, 57	43.5–49	−2 to 2	48–70	9.3
48.5, 20	48 –50	−1 to 1[b]	16–24	12
50.5, 53	49 –54	−3 to 4	36–66	5.6
52, 24	50 –54	−2 to 3	18–30	1.9
55.5, 38	54 –57	−2 to 2	30–46	6.1
57.5, 35	57 –59	−2 to 2	27–43	3.9
58, 18	56 –59.5	−10 to 7	9–23	1.4
62.5, 26	60 –64	−4 to 3	20–35	2.6
64.5, 20	64 –66	−5 to 4	15–25	2.1
70, 11	59.5–80	−10 to 5	5–15	0.5

[a] The kinematic distance based on H I peak velocity differs slightly from the CO kinematic distance.

[b] Because of the prominence of high-latitude local emission from this longitude-velocity range, the latitude range for this distant cloud has been arbitrarily set equal to −1 to 1, which corresponds to a cloud thickness of 400 pc.

variations when integrated over latitude, as on an (l, v) diagram. The self-absorbing cloud associated with M17, for example (Sato and Fukui 1978), is readily observed on the (l, b) diagram in Figure 2 (at $v = 20$ km s^{-1}, $l = 15°$ and $b = -0.^{\circ}25$), but this emission minimum does not show up prominently on the (l, v) diagram in Figure 1, where the emission-line cloud is centered at $(l, v) = (12, 14)$. The absorption error could be important in other regions, however, especially where a CO cloud is to the side of the nearest H I emission (cf. § IV).

Other identification errors can be produced by velocity crowding, Galactic-scale streaming motions, and near-far kinematic distance blending, especially near the terminal velocity curve on the (l, v) diagram, and near the intersection points of the spiral arms. Such errors are discussed in § V. Fortunately, the bright H I gas is so highly clumped into clouds and spiral arms that line-of-sight blending errors turn out to be infrequent. Also, the (l, v) coordinates where these errors occur are known, so the potentially blended emission regions can be avoided in general discussions of cloud properties (as in §§ VI and VII).

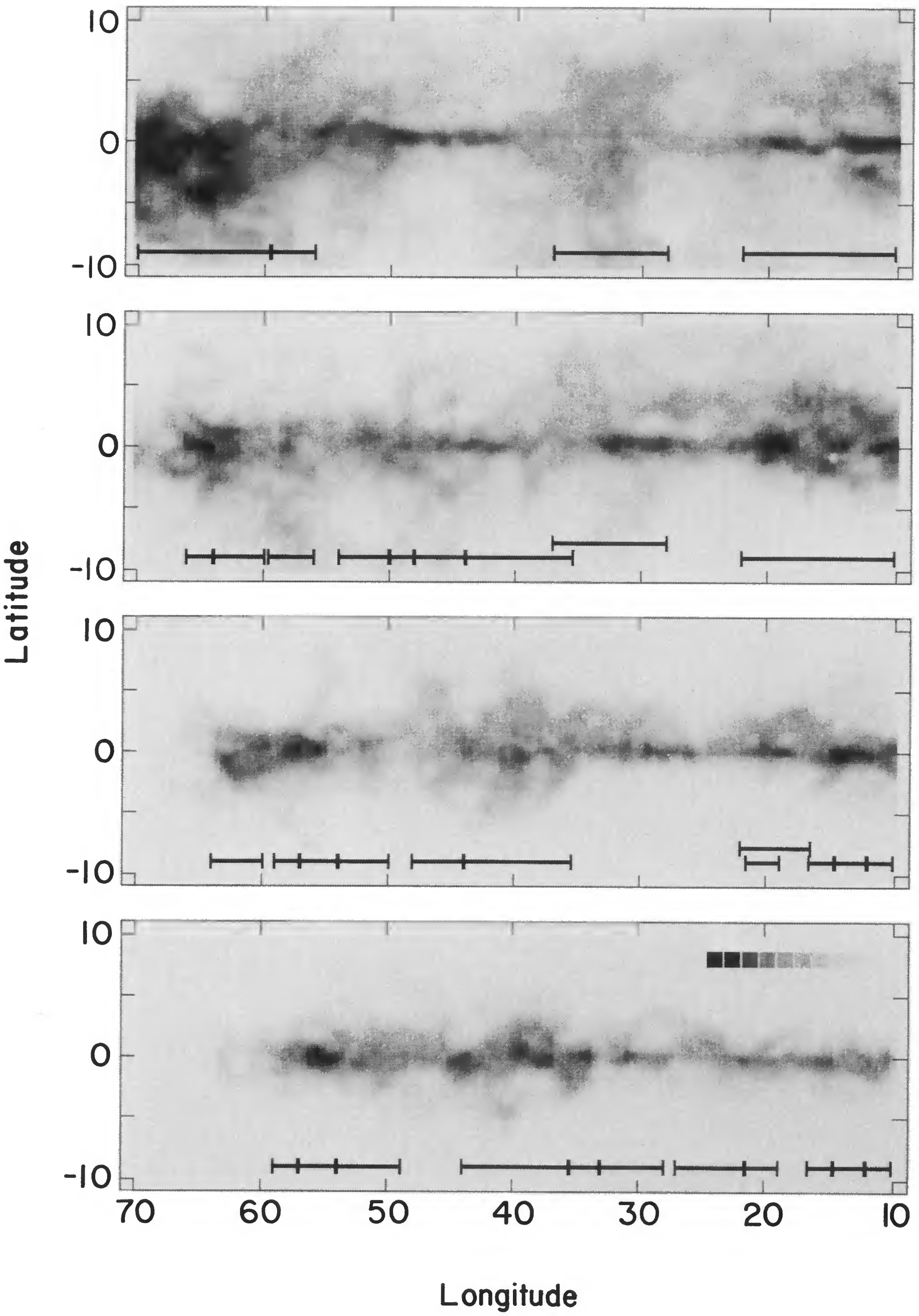

FIG. 2a

FIG. 2.—Sky maps of the antenna temperature of 21 cm emission from the Weaver and Williams (1973) survey. Each map is for a single velocity channel, of width 2.11 km s^{-1}. Gray scale boxes start at 20 K for the lightest shade and increase in increments of 10 K up to 100 K. Bracketed lines in each plot indicate the longitude ranges of the clouds identified in Fig. 1c and in Table 1. Velocities range from 10 km s^{-1} to 100 km s^{-1} in steps of 10 km s^{-1}; (a) 10 km s^{-1} (*top*) to 40 km s^{-1} (*bottom*); (b) 50 km s^{-1} (*top*) to 70 km s^{-1} (*bottom*); (c) 80 km s^{-1} (*top*) to 100 km s^{-1} (*bottom*).

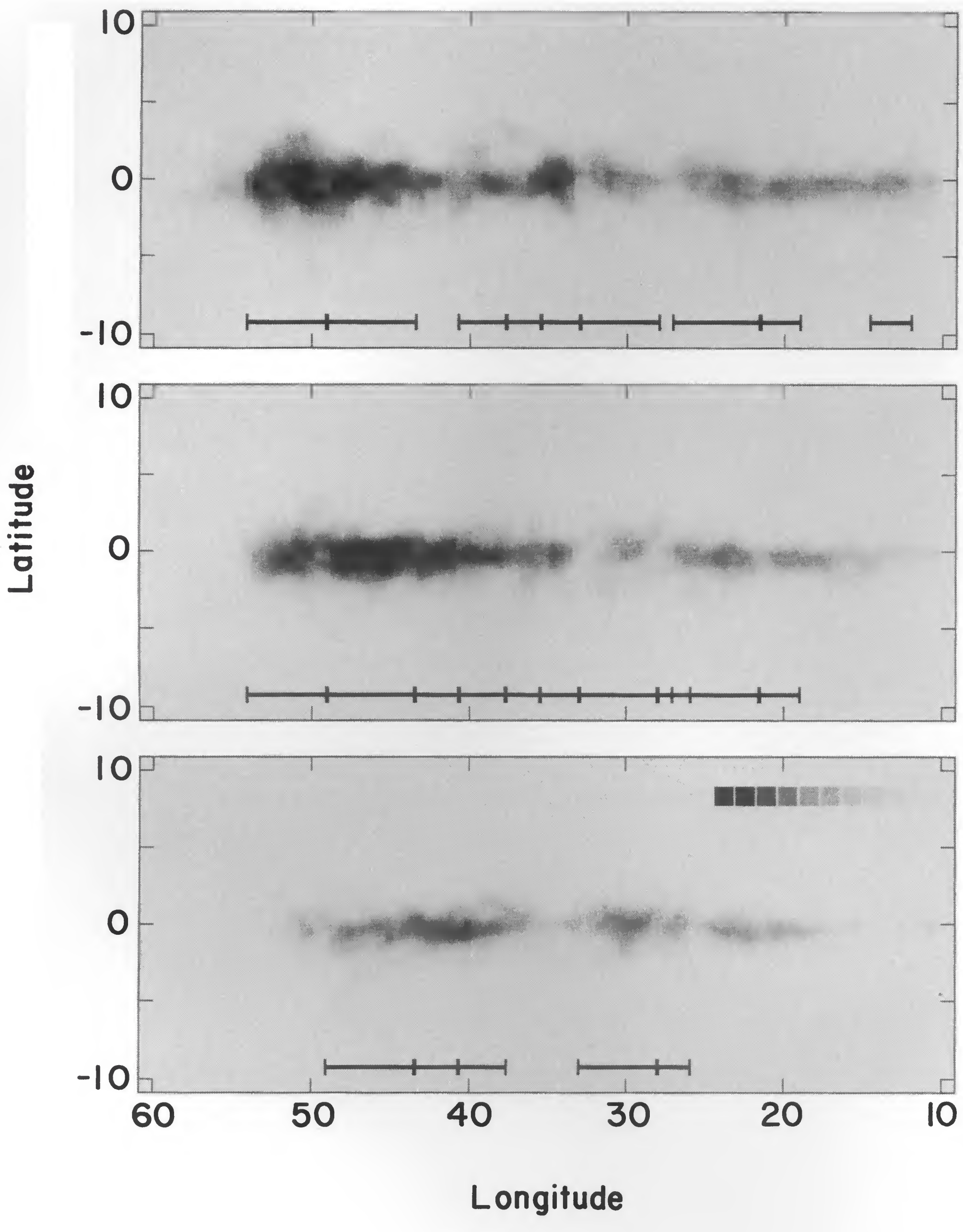

FIG. 2b

ELMEGREEN AND ELMEGREEN (*see* **320**, 184)

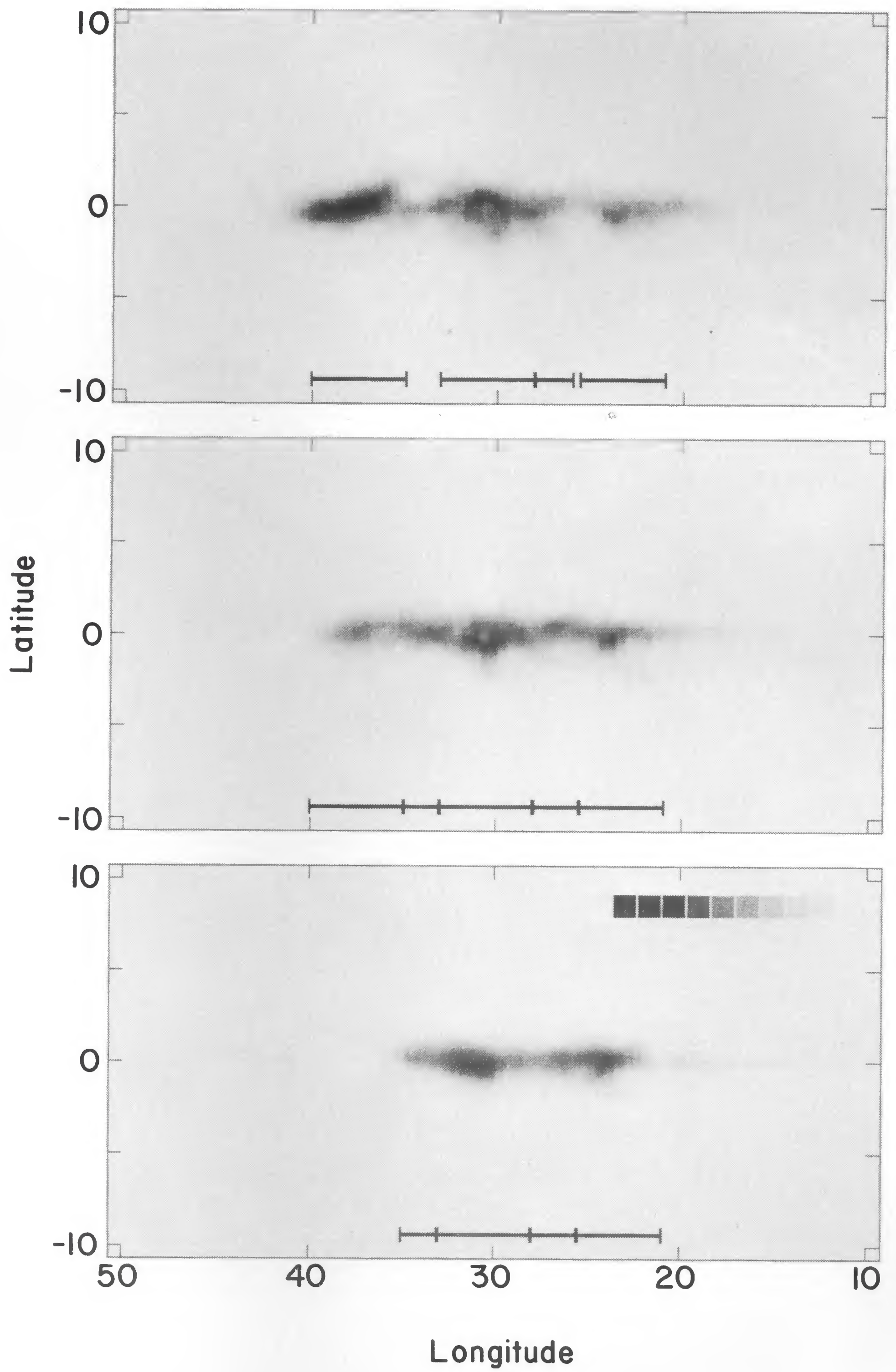

FIG. 2c

ELMEGREEN AND ELMEGREEN (*see* **320**, 184)

III. H I MASSES

a) Uniform Cloud Model

Estimates for the H I mass enclosed in each identifying rectangle are in Table 2. Column (1) is the cloud coordinate from Table 1. The masses in columns (2), (3), and (4), $M_{\rm uniform}$, were calculated from the equation

$$M = K\mu D(l, v)^2 \int_{v_{\min}}^{v_{\max}} \int_{l_{\min}}^{l_{\max}} \int_{b_{\min}=-10°}^{b_{\max}=10°} T_{\rm mass}\, db\, dl\, dv \;, \tag{3}$$

where M is the mass in grams, $K = 1.82 \times 10^{18}$ (cm^2 deg km s^{-1})$^{-1}$, $\mu = 2.2 \times 10^{-24}$ g is the mean atomic weight including helium and heavy elements, D is the distance in centimeters, $T_{\rm mass} = N/(K\Delta v)$ is a measure of the column density, N, per unit velocity, Δv, and is given as an effective brightness temperature for an equivalent column of optically thin emission, and dl and dv range over the longitudes and velocities in Table 1. Column (2) is the mass calculated for emission clipped at 40 K, and column (3) is for unclipped emission. The masses in columns (2) and (3) assume that the clouds are optically thin,

TABLE 2

ATOMIC CLOUD MASSES ($\times 10^6\ M_\odot$)

	$M_{\rm uniform}$			$M_{\rm clump}$		
(l, v) (°, km s^{-1}) (1)	$T_s = \infty$ (2)	∞[a] (3)	120 K (4)	$T_i = 10^3$ K (5)	120 K (6)	$M_{\rm abs}$ (7)
10.5, 33	1.0	2.0	2.0	2.4	2.6	0.0
12, 6	0.04	0.04	0.06	0.07	0.08	0.05
12, 14	3.4	4.9	6.59	7.8	8.7	2.3
13.5, 32	1.4	2.5	2.83	3.3	3.8	2.8
13.5, 47	0.88	1.9	1.52	1.9	2.0	0.0
15, 28	0.92	1.6	1.71	2.0	2.3	0.0
19.5, 42N	1.3	2.3	2.20	2.7	2.9	3.3
19.5, 42F	1.4	2.6	2.42	2.9	3.2	3.6
23, 54N	1.6	3.3	2.69	3.3	3.6	0.0
23, 54F	1.9	3.9	3.23	3.9	4.3	0.0
24, 102N	2.8	6.0	4.86	5.9	6.4	8.8
24, 102F	1.7	3.6	2.96	3.6	3.9	5.4
26, 105	1.9	4.2	3.29	4.0	4.4	0.0
27, 64	0.47	1.2	0.77	0.95	1.0	0.0
30, 78	2.6	5.5	4.66	5.6	6.2	2.6
30.5, 94	3.7	6.4	6.72	8.1	8.9	2.2
31, 47N	0.27	0.66	0.47	0.58	0.62	0.27
31, 47F	2.0	4.8	3.44	4.2	4.6	2.0
31.5, 13N	0.32	0.48	0.54	0.66	0.71	0.65
31.5, 13F	7.1	10.5	11.81	14.5	15.6	14.2
34, 50	0.99	1.7	1.93	2.3	2.6	1.8
34, 95	1.5	2.9	2.54	3.1	3.4	1.5
36, 58	5.1	10.0	9.71	11.5	12.9	0.0
37.5, 81	5.3	9.1	9.83	11.7	13.0	0.0
39.5, 33	2.4	4.0	4.43	5.3	5.9	6.5
40, 64	11.4	18.5	23.66	26.9	31.4	8.8
41, 62	7.5	10.6	17.65	18.9	23.4	31.5
46, 28	0.44	0.8	0.75	0.92	1.0	0.0
47.5, 57	14.4	22.0	36.35	37.8	48.1	0.0
48.5, 20	5.84	11.2	10.4	12.6	13.8	1.6
50.5, 53	7.3	11.3	14.93	17.1	19.8	3.5
52, 24	0.25	0.53	0.43	0.53	0.57	0.0
55.5, 38	2.5	4.9	5.00	5.8	6.6	1.3
57.5, 35	0.74	1.4	1.44	1.7	1.9	0.0
58, 18	0.38	0.55	0.65	0.8	0.87	0.0
62.5, 26	0.75	1.3	1.43	1.7	1.9	1.6
64.5, 20	0.29	0.46	0.59	0.68	0.78	0.07
70, 11	0.24	0.30	0.58	0.62	0.77	0.31

[a] This column is for unclipped emission; all other columns are for emission clipped at 40 K.

in which case the spin temperature is $T_s = \infty$ and

$$T_{\rm mass} = T_{40}/\eta \quad \text{and} \quad T_{\rm mass} = T_A/\eta \;, \tag{4}$$

for clipped (col. [2]) and unclipped (col. [3]) emission, respectively; the beam efficiency is $\eta = 0.85$ (Weaver and Williams 1973). The masses in column (4) assume that the clouds are uniform and at a spin temperature of $T_s = 120$ K, in which case

$$T_{\rm mass} = -T_s \ln\,[1 - (T_{40}/\eta T_s)] \tag{5}$$

for clipped emission. These column (4) masses correct for H I opacity in a simple way, because the observed brightness temperature from a uniform cloud is $T_B = T_s(1 - e^{-\tau})$ for optical depth $\tau = N/(KT_s\,\Delta v) = T_{\rm mass}/T_s$.

b) Clumpy Cloud Model

The masses in columns (5) and (6), $M_{\rm clump}$, are corrected for H I opacity by assuming that each cloud is a complex of large unresolved clumps that are immersed in an interclump medium. This is similar in some respects to the model by Baker and Burton (1975). The present method uses an analytic solution to the radiative transfer equations, applied to a relatively small distance on the line of sight, and the clump velocities are assumed to be random. Baker and Burton (1975) used a Monte Carlo approach and applied it to a long line of sight, on which the average clump velocity varies systematically because of Galactic shear.

The masses of the H I complexes are determined by integrating a *derived* column density over the lines of sight and velocities contained within the cloud boundaries. This column density was derived as follows. The total column density in a velocity sampling interval of width $\Delta v(=1.05$ km s^{-1}, or half the spectral channel width of 2.11 km s^{-1}) is denoted by ΔN. If the average ratio of the interclump mass to the clump mass equals I, then the average interclump column density in a velocity sampling interval is $I\Delta N/(1 + I)$, and the average column density in clumps is $\Delta N/(1 + I)$. The optical depth, temperature, and line width of a clump are assumed to equal τ_c, T_c, and Δv_c, so the total column density in a single clump is $N_c = K\tau_c\, T_c\, \Delta v_c$, and the column density from a clump in a velocity channel is $N_c\, \Delta v/\Delta v_c$. This implies that the expected number of clumps in a velocity interval is

$$\epsilon = \frac{\Delta N \Delta v_c}{(1 + I)N_c\, \Delta v} = \frac{\Delta N}{(1 + I)K\tau_c\, T_c\, \Delta v} \;. \tag{6}$$

The interclump temperature is T_i, so the opacity of the interclump medium in a velocity channel equals

$$\tau_i = \frac{I\Delta N}{(1 + I)KT_i\,\Delta v} \;. \tag{7}$$

The radiative transfer solution derived in Appendix A (eq. [A10]) gives the expected H I brightness temperature, T_B, for a single velocity channel in terms of the clump and interclump temperatures and opacities, and the expected number of clumps in a channel:

$$T_B = T_c + [T_i(1 - e^{-\tau_i}) - T_c]\,\exp\,[-\epsilon(1 - e^{-\tau_c})] \;. \tag{8}$$

Because τ_i and ϵ depend on ΔN, the column densities that give the observed brightness temperatures can be derived from equations (6)–(8). The total cloud mass can then be obtained from equation (3), using $T_{\rm mass}(l, b, v) = \Delta N(l, b, v)/(K\Delta v)$. As for the other temperature-clipped masses, only the lines of sight and velocity channels with antenna temperatures greater than 40 K were considered in these mass integrals.

The parameters for clumpy clouds are modeled after the H I emission from large atomic clouds and warm intercloud gas in the solar neighborhood. The clumps are taken to have a spin temperature $T_c = 120$ K, an optical depth $\tau_c = 1$, and a velocity full-width $\Delta v = 4$ km s^{-1}. This clump temperature is typical, or possibly high, for local diffuse clouds; many clumps could be at lower temperatures, especially if cold molecular matter is present. The value of 120 K is probably an upper limit, giving a lower limit to the cloud mass. The line width of 4 km s^{-1} is the average for each of the samples of H I clouds studied by Lazareff (1975) and Crovisier (1981). The assumed H I opacity in the clumps, $\tau_c = 1$, corresponds to a column density of 8.7×10^{20} cm^{-2} for a temperature of 120 K and a line width of 4 km s^{-1}. Such a cloud has a color excess of $E(B-V) = 0.12$ mag. It corresponds to approximately the geometric mean between Spitzer's (1985) "diffuse" ($N = 3.5 \times 10^{20}$ cm^{-3}) and "large" ($N = 1.7 \times 10^{21}$ cm^{-3}) H I clouds. Smaller clump opacities, such as $\tau_c = 0.3$ for small diffuse clouds (e.g., Crovisier 1981) produce such a uniform intensity that the total cloud masses are similar to those calculated for a uniform cloud with the same spin temperature (see Appendix B).

The interclump medium is assumed to have a spin temperature of at least $T_i = 1000$ K for column (5) in Table 2 and $T_i = 120$ K for column (6); the interclump mass is taken equal to the factor $I = 0.5$ times the total clump mass. An interclump temperature >1000 K is characteristic of the warm intercloud medium (Davies and Cummings 1975; Mebold and Hills 1975; Lazareff 1975; Dickey, Salpeter, and Terzian 1979; Mebold *et al.* 1982; Payne, Salpeter, and Terzian 1983; Listzt 1983; Kulkarni and Heiles 1987). Although the local intercloud medium may be much warmer than 1000 K, possibly exceeding 10 times this in some regions, the interclump medium in a giant cloud complex might be cooler than the local value because the interclump density inside a complex could be larger than the local intercloud density. Fortunately this temperature does not significantly affect the mass determination because at temperatures larger than or equal to 1000 K, the interclump medium in the model is optically thin. The insensitivity of the masses to $T_i > 1000$ K is illustrated in Appendix B. The case with $T_i = 120$ K, used for column (6) in Table 2, is taken to be representative of an interclump medium composed of many small diffuse clouds. The temperature of 120 K is probably a lower limit.

A simple model that illustrates the scaling of the derived cloud mass with the assumed parameters is discussed in Appendix B. The result is relatively insensitive to the interclump temperature; it depends more strongly on the assumed clump opacity and interclump mass fraction.

c) *Absorption-Line Masses*

The masses in column (7) of Table 2 are estimates based on the average 21 cm absorption opacity determined from numerous background continuum sources. Table 3 lists these background sources and their directions, and it gives the observed absorption-line velocities, v, opacities, τ, and emission temperatures, T_E. The derived spin temperatures, T_s, corrected for beam efficiency, and the products $K\tau T_s$ are also tabulated. To estimate the H I cloud masses, the average column density per km s^{-1}, $K\tau T_s$, was derived for each H I cloud, and this average was multiplied by the cloud area, πR^2, and by twice the cloud velocity dispersion, for cloud radius R and dispersion σ listed in Table 5 below.

The absorption-line measurements are probably inaccurate, especially for the single-dish observations. They are considered here only as a crude check on the masses derived by other means, and are considered to be accurate only to the nearest order of magnitude. Table 3 primarily illustrates the presence of narrow absorption features inside the complexes, and this seems to justify the clumpy cloud model and the clump parameters chosen for it.

d) *Resolving the Near/Far Distance Ambiguity*

The H I masses of clouds that contain CO features at both the near and far kinematic distances were determined by dividing the total 21 cm flux into two parts whose corresponding masses are proportional to the molecular masses at these distances. The resulting near and far H I masses are listed separately in Table 2. They are very uncertain.

The blending of near and far kinematic distances occurs primarily where the inner three spiral arms intersect (see §§ V and VII). Other locations on the (l, v) diagram appear to have no severe distance ambiguity. This fortunate circumstance results from the clumpy distribution and spiral arm confinement of the gas (as first recognized from the CO emission—Dame *et al.* 1986). Aside from the spiral arm intersection points, most locations on an (l, v) diagram have well-determined distances. The largest distance errors occur near the terminal velocity curve, where the kinematic distance may be too large or small by 50%.

e) *Discussion of Cloud Masses*

Table 2 indicates that the masses derived for the clumpy cloud model are larger than the masses derived for the uniform cloud model with the same excitation temperature for the cool gas. This mass difference may be understood as follows. A uniform cloud with a certain column density has an equal brightness temperature all across its projected surface. A clumpy cloud with the same average column density is mottled in appearance, with some lines of sight brighter than others, depending on the locations of the clumps (see, for example, Fig. 4 in Jenkins 1970). The lines of sight with fewer than average clumps will have less than the average brightness temperature, and the lines of sight with more than the average number of clumps will have greater than the average brightness temperature. Because the brightness temperature increases with the total column density ΔN approximately as $1 - e^{-\Delta N/(KT_c \Delta v_c)}$, the deficit in brightness temperature in the clump-poor lines of sight is greater than the excess in brightness temperature in the clump-rich lines of sight. The result is an average brightness temperature for a clumpy cloud that is less than the average brightness temperature for a uniform cloud at the same total column density. Thus a greater column density and a greater total cloud mass are required for a clumpy cloud to give the same brightness temperature as a uniform cloud.

The absorption line studies give masses that are similar to the other H I masses, but, of course, the absorption-line masses are very inaccurate. The real importance of the absorption lines is that they indicate that each H I cloud complex contains numerous cool clumps. The opacities and spin temperatures listed in Table 3 justify the parameter assumptions ($\tau_c \approx 1$, $T_c \approx 120$ K) for the derivation of mass in the clumpy cloud model.

1987ApJ...320..182E

TABLE 3

H I ABSORPTION MEASUREMENTS

(l, v) (°, km s^{-1})	Source	l	b	v (km s^{-1})	τ	T_E (K)	T_s (K)	$K\tau T_s$ ($\times 10^{20}$ cm^{-2} / km s^{-1})	References
12, 6	W33	12°7	−0°8	4	0.5	90	318	2.9	1
	NRAO 572	25.4	−0.16	5	1.5	60	107	3.0	1
	1817−098	20.7	2.3	8	2	60	69	2.5	2
	1819−131	17.9	0.4	6	1.6	65	81	2.4	2
	1819−096	21.0	2.0	4	2	50	57.8	2.1	2
	1829−106	21.3	−0.6	5	2	60	69	2.5	2
12, 14	1817−098	20.7	2.3	25	1	60	95	1.7	2
	1819−131	17.9	0.4	20	1.4	100	133	3.4	2
	1819−096	21	2	19	0.7	65	129	1.6	2
	1819−096	21	2	30	2	70	81	3.0	2
	1829−106	21.3	−0.6	18	0.6	72	160	1.8	2
	1755−16	12.43	3.8	21.2	0.67	71	145	1.8	3
	1811−16	13.87	0.24	20	1.61	106.7	133	3.9	3
	1819−09	21.06	1.94	19.8	0.34	20.4	70.3	0.44	3
	P1730−13	12.0	10.8	14	0.3	15	80	0.44	4
	W33	12.7	−0.8	20	4	60	85	6.2	1
13.5, 32	1811−16	13.87	0.24	45	1.61	106.7	133	3.9	3
	W33	12.7	−0.8	35	3	100	146	8.0	1
19.5, 42	1819−096	21	2	30	2	70	81	3.0	2
	1819−096	21	2	50	0.3	10	39	0.21	2
	1829−106	21.3	−0.6	40	1.4	72	96	2.5	2
	1829−106	21.3	−0.6	55	1.6	50	63	1.8	2
	1819−09	21.06	1.94	32.6	∞	2.2	47.5	∞	3
	NRAO 572	25.4	−0.16	40	1	70	154	2.8	1
	NRAO 572	25.4	−0.16	60	2	85	137	5.0	1
24, 102	NRAO 572	25.4	−0.16	90	2	95	153	5.6	1
	1829−106	21.3	−0.6	80	1.2	55	79	1.7	2
30, 78	1838−01	30.12	1.37	62	1.51	34.9	45	1.2	3
30.5, 94	1838−01	30.12	1.37	90	0.36	34.9	116	0.76	3
31, 47	1838−01	30.12	1.37	50	0.48	48.5	127	1.1	3
31.5, 13	1849+005	33.5	0.2	15	2	75	87	3.2	2
	1821+01	31.42	6.91	16.6	0.87	50.9	88	1.4	3
	1838−01	30.12	1.37	13	0.87	63	109	1.7	3
	1859+03	37.2	−0.6	13.52	1.8	…	…	…	5
	1900+01	35.7	−1.9	11.82	1.04	…	…	…	5
34, 50	1849+005	33.5	0.2	38	1.6	75	94	2.7	2
	1849+005	33.5	0.2	45	1.6	85	107	3.1	2
	1849+005	33.5	0.2	50	1.2	100	143	3.1	2
	1849+005	33.5	0.2	55	1.7	85	104	3.2	2
34, 95	1849+005	33.5	0.2	92	1.5	60	77	2.1	2
	1849+005	33.5	0.2	102	1.2	88	126	2.8	2
36, 58	1859+03	37.2	−0.6	54.65	0.49	…	…	…	5
	1859+03	37.2	−0.6	62.43	0.75	…	…	…	5
37.5, 81	1859+03	37.2	−0.6	79.12	0.99	…	…	…	5
39.5, 33	1900+01	35.7	−1.9	32.09	2.2	…	…	…	5
	1900+01	35.7	−1.9	39	0.8	…	…	…	5
	1843+098	41.1	5.8	25	0.3	37	143	0.78	2
	1909+049	39.7	−2.2	30	1.7	70	86	2.7	2
	1910+052	40.1	−2.3	30	0.8	70	127	1.9	2
	1915+062	41.6	−2.9	30	0.5	60	152	1.4	2
	1843+09	41.11	5.77	27	0.24	30.7	146	0.64	3
	W49A	43.1	0.2	38	3	105	153	8.4	1
	1859+03	37.2	−0.6	41.25	1.14	…	…	…	5
	1857+12	45.4	4.15	30	0.25	47.8	217	0.99	3
40, 64	1909+049	39.7	−2.2	50	0.5	45	114	1.0	2
	1910+052	40.1	−2.3	54	0.8	38	69	1.0	2
	1910+052	40.1	−2.3	70	0.2	41	226	0.82	2
41, 62	W49A	43.1	0.2	60	4	105	149	10.9	1
48.5, 20	1909+161	49.7	2.9	22	0.35	40	135	0.86	2
	W51	49.4	−0.38	19	0.6	50	154	1.7	1
50.5, 53	1909+161	49.7	2.9	55	0.04	39	994	0.72	2
	W51	49.4	−0.38	40–70	2	0	…	…	1
55.5, 38	1923+210	55.6	2.3	40	0.15	34	244	0.67	2
58, 18	1919+21	55.8	3.5	9.59	146	…	…	…	5
62.5, 26	1950+253	62.4	−1	25	1	100	158	2.9	2
64.5, 20	1922+33	66.39	8.38	23.7	0.43	14.4	41	0.32	3
70, 11	1950+253	62.4	−1	15	1.1	100	150	3.0	2
	2007+249	64.0	−4.3	10	1.6	106	133	3.9	2
	1958+25	63.71	−2.31	11.1	1.14	81.5	120	2.5	3
	2012+23	63.4	−6.12	14.4	1.02	67.6	106	2.0	3
	2012+26	65.92	−4.58	13.5	1.43	104.4	137	3.6	3
	2018+23	64.02	−7.53	11	0.92	60.7	101	1.7	3
	3C409	63.4	−6.1	15.4	0.85	17.6	31	0.48	6
	3C409	63.4	−6.1	13.2	0.96	34.0	55	0.96	6

REFERENCES.—(1) Dickey and Benson 1982; (2) Dickey *et al.* 1983; (3) Crovisier, Kazès, and Aubry 1978; (4) Lazareff 1975; (5) Dickey *et al.* 1981; (6) Mebold *et al.* 1982.

A conservative lower limit for the mass of a giant H I cloud is the mass that is calculated for the uniform case with $T = 120$ K using the clipped emission (Table 2, col. [2]). This is a lower limit because clumpiness and a lower spin temperature increase the cloud mass. A better H I mass is probably the clumpy cloud mass listed in columns (5) or (6) of Table 2. This mass is also a lower limit because a substantial amount of cold molecular material is present inside most of the clouds (§ IV), and this molecular material probably has cold H I. Peripheral H I emission, omitted by the clipping procedure, may also add to the total cloud mass. The mass of the peripheral emission is essentially the difference between the masses in columns (3) and (2) in Table 2, because opacity corrections are probably small for this low-brightness gas. The H I masses used in the following discussions of molecular fractions and gravitational self-binding are from the clumpy cloud model with the warm intercloud medium (col. [5]).

The H I masses in Table 2 have a differential distribution function that varies as $n(M) \propto M^{-1}$ to M^{-2} between 10^6 and several times 10^7 $M_{\odot}$. Considering the inaccuracies of the mass determinations and the cloud identification procedures, this is not significantly different from the mass distribution function for molecular clouds (e.g., Dame *et al.*, 1986). As for the molecular clouds, most of the atomic mass is distributed among the largest complexes. But because the continuation of the mass spectrum to lower masses is not known from the present study, the atomic cloud mass distribution function need not be a power law, as it is for molecular clouds.

IV. ASSOCIATIONS BETWEEN H I AND CO CLOUDS AND THE MOLECULAR MASS FRACTION

The longitudes and velocities of the CO emission features in Dame *et al.* (1986) and Myers *et al.* (1986) are indicated by bracketed lines in Figure 3 (Plate 8). The brackets enclose the longitude ranges for each cloud given by Myers *et al.* (1986), and the velocity extents of the brackets are ± 2 km s^{-1}. Clouds at the near distance are represented by single vertical lines, clouds at the far distance, by double lines, and clouds with components at both near and far distances, by triple lines. Clouds with H_2 masses in excess of 10^6 $M_{\odot}$ are denoted by thick lines, and clouds with smaller masses by thin lines.

Table 4 lists the CO complexes that appear to be associated with the H I features. In some cases the association is ambiguous because CO is to the side of the H I. The molecular masses

TABLE 4

GIANT MOLECULAR CLOUDS ASSOCIATED WITH H I COMPLEXES

(l, v) (°, km s^{-1}) (1)	$(l, v)_{CO}$ (°, km s^{-1}) (2)	$M(H_2)$ ($\times 10^6$ $M_{\odot}$) (3)	M_{total} ($\times 10^6$ $M_{\odot}$) (4)	$M(H_2)/M_{total}$ (5)
10.5, 33	...[a]	...	2.4	...
12, 6	...	...	0.1	...
12, 14	(14, 20)(17, 22)(20, 25)	1.4	9.2	0.16
13.5, 32	...	...	3.3	...
13.5, 47	(12, 45)(13, 54)	4.0	5.8	0.68
15, 28	(14, 39)(17, 44)	3.2	5.2	0.61
19.5, 42N	(18, 48)(20, 42)	1.7	4.3	0.36
19.5, 42F	(21, 60)	2.0	4.9	0.41
23, 54N	(24, 42)(25, 55N)(22, 53)	3.0	6.3	0.48
23, 54F	(25, 55F)	4.0	8.0	0.50
24, 102N	(23, 78N)(24, 98)(24, 110)	13.0	18.9	0.69
24, 102F	(23, 78F)	10.0	13.6	0.73
26, 105	...	...	4.0	...
27, 64	(26, 65)	0.32	1.3	0.25
30, 78	(29, 80)	5.0	10.7	0.47
30.5, 94	(31, 95)	10.0	18.1	0.55
31, 47N	(29, 52)	0.25	0.8	0.30
31, 47F	(31, 48)	4.0	8.2	0.49
31.5, 13N	(31, 12)(35, 13)	0.041	0.7	0.055
31.5, 13F	(33, 10)	1.0	15.5	0.065
34, 50	(35, 44)	1.1	3.4	0.33
34, 95	...	...	3.1	...
36, 58	(36, 57)	5.0	16.5	0.30
37.5, 81	(37, 82)	10.0	21.7	0.46
39.5, 33	(39, 32)(39, 42)(41, 37)	0.28	5.6	0.047
40, 64	(40, 59)	6.3	33.2	0.19
41, 62	(43, 63)	5.0	24.0	0.21
46, 28	(46, 25)	0.016	0.9	0.017
47.5, 57	(44, 60)(46, 59)	4.7	42.6	0.11
48.5, 20	(49, 18)	0.4	13.0	0.03
50.5, 53	(49, 59)(50, 45)(51, 55)(53, 60)	2.3	19.4	0.12
52, 24	(53, 24)	0.04	0.6	0.070
55.5, 38	(56, 36)(54, 40)	0.70	6.5	0.11
57.5, 35	(58, 37)	0.16	1.8	0.086
58, 18	...	...	0.80	...
62.5, 26	(60, 27)	0.08	1.8	0.045
64.5, 20	...	...	0.7	...
70, 11	...	...	0.6	...

[a] No cataloged H_2 mass.

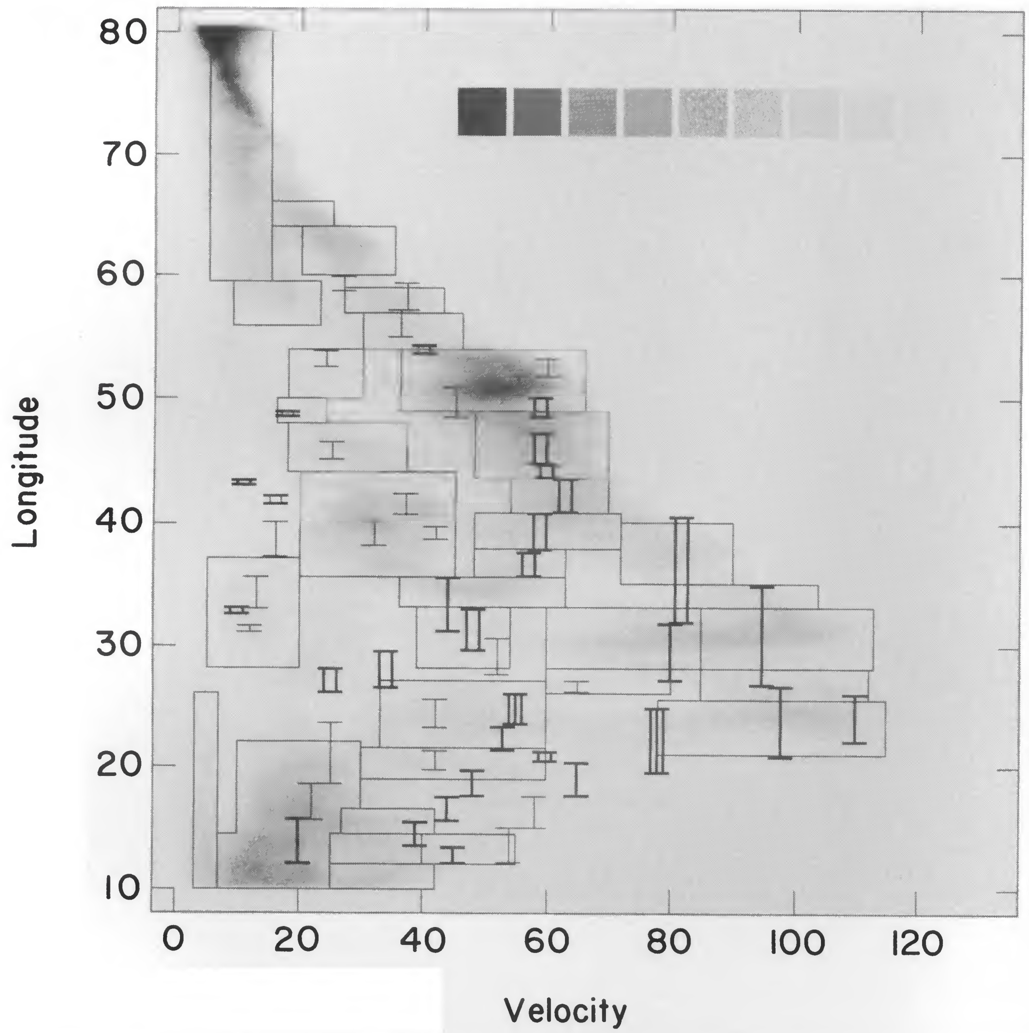

FIG. 3.—Gray scale representation of 21 cm emission, from Fig. 1*c*, with bracketed lines indicating the longitude ranges and centroid velocities of prominent CO emission from Dame *et al.* (1986) and Myers *et al.* (1986). Clouds at the near kinematic distance are represented by single vertical lines, clouds at the far distance by double lines, and clouds with components at both near and far distances, by triple lines. Clouds with H_2 masses in excess of $10^6\ M_\odot$ are denoted by thick lines, and clouds with smaller masses, by thin lines.

are from Myers *et al.* (1986). The atomic mass of each cloud is from column (5) in Table 2, and the total complex mass is the sum of the atomic and molecular masses. The molecular mass fraction, equal to the ratio of the molecular mass to the total mass, is in column (5).

Figure 4 plots the molecular mass fraction versus the distance from the galactic center for all of the H I complexes that contain cataloged giant molecular cloud complexes. There is a strong correlation. Apparently the *average* radial variation in the molecular mass fraction of interstellar gas, found in previous studies (Scoville and Soloman 1975; Gordon and Burton 1976), is partly the result of this real variation in individual cloud complexes. The figure also suggests that the molecular fraction of giant H I clouds beyond the solar circle should be very small. This is consistent with the results of Grabelsky (1985), who finds that, in the outer part of the Carina arm, H I clouds with $10^7\ M_\odot$ (McGee and Milton 1964) contain CO clouds with total molecular masses of $10^5\ M_\odot$ to $10^6\ M_\odot$.

The average molecular fraction within 1 kpc of the Sun is $\sim$17%, for an average H_2 density of 0.1 cm^{-3} (Dame *et al.* 1987) an an overall H density from extinction of 1.2 cm^{-3} (Spitzer 1978). This local fraction exceeds the extrapolation of the correlation in Figure 4. There are several reasons for this difference. First of all, the Sun is apparently not inside a supercloud at the present time, so the molecular fraction in the solar neighborhood should not necessarily be the same as the extrapolated molecular fraction for individual clouds. (The Sun is apparently inside an old and unbound supercloud complex, which presumably began to form the stars in Gould's Belt 6×10^7 yr ago when the solar neighborhood was in the crest of the Sagittarius-Carina spiral arm. Our subsequent emergence from this arm has presumably led to the tidal disruption of this complex—see § VII*c*.) Second, the CO masses of the nearest cloud complexes in Figure 4, which are the ones at a galactocentric distance of $\sim$9 kpc, could be systematically understimated compared to the CO masses of more distant clouds, because the local clouds sometimes extend beyond the 2° boundary of the CO survey, and so are not fully measured. Third, the CO temperature-clipping procedure used by Myers *et al.* (1986), which attempts to eliminate small clouds in the foreground or background of the large clouds under study, will underestimate the masses of nearby clouds that are well resolved. Corrections for these latter two effects could increase the molecular fractions of the cloud complexes between 8 and 9 kpc in the figure, possibly by a factor between 1.5 and 2, which would then bring their values closer to a simple linear extrapolation of the molecular fractions inside 7 kpc, and somewhat closer to the value in the solar neighborhood.

Of course, the molecular fraction for individual small clouds in the solar neighborhood need not be the same as the molecular fractions for the large clouds studied here. Nearby small clouds that are well resolved have molecular cores and rela-

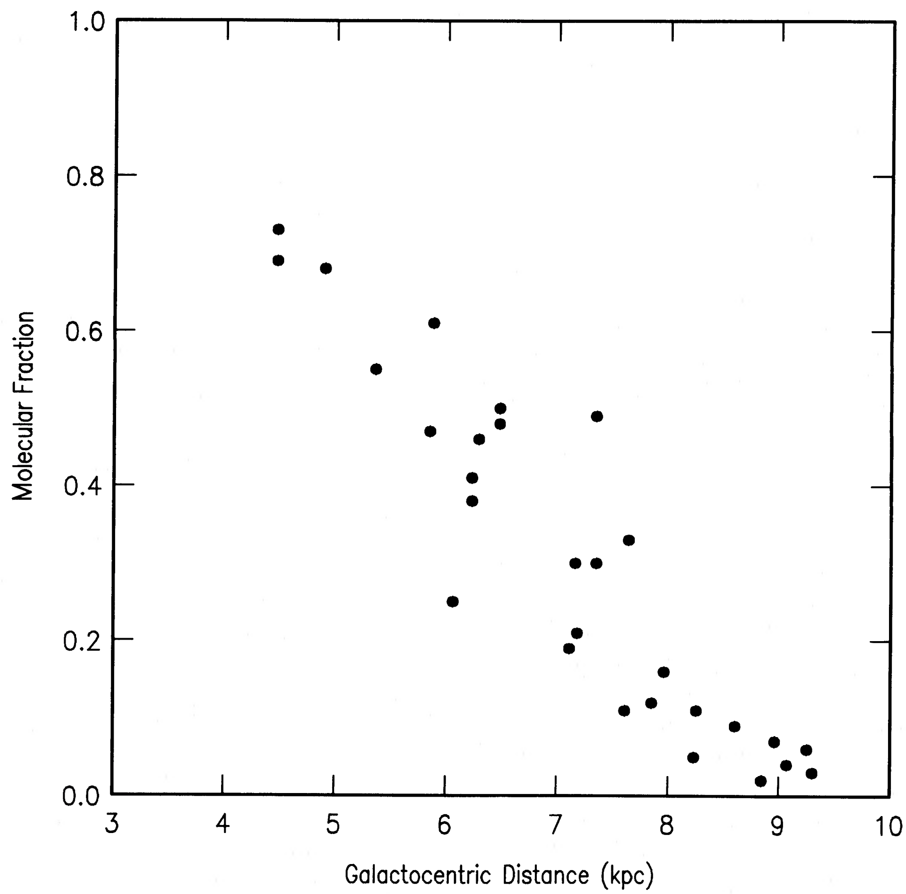

FIG. 4.—The molecular mass fraction vs. the distance from the Galactic center (with the Sun's distance equal to 10 kpc) for clouds with cataloged molecular components. The atomic cloud masses are from col. (5) in Table 2. The correlation in this figure suggests that the observed variation in the *average* molecular fraction of interstellar gas may be the result of a variation in the molecular fraction inside individual cloud complexes (cf. § IV).

tively small H I emission envelopes (see references in § I), so the molecular fraction in each distinct cloud is large. The overall molecular fraction on the scale of several hundred parsecs should be less than this because neutral hydrogen is present between the CO clouds. The interstellar medium appears to be hierarchically clumped (e.g., Scalo 1985), so the molecular fraction of any particular region should depend on the level of the hierarchy. Figure 4 is intended to include only the largest hierarchy. Comparisons to molecular fractions derived for other levels in the hierarchy (to local molecular clouds, for example) should not give the same fractions.

The basic conclusion drawn from Figure 4 is that the molecular fraction in individual cloud complexes decreases systematically with increasing galactocentric distance, in a way that might explain the observed decrease in the *average* molecular fraction, determined previously for whole annuli around the Galactic center. This change in the molecular fraction occurs even though the masses of the individual clouds does not change much with galactocentric distance. The clouds in both the first quadrant studied here and in the fourth quadrant studied by Grabelsky *et al.* (1987) all contain around $10^7\ M_\odot$, regardless of galactocentric distance. Thus, the *average* molecular fraction of the interstellar gas does not decrease with galactocentric distance because the fundamental cloud mass is decreasing. The average fraction decreases because the molecular cores becomes less massive, and the atomic envelopes become more massive, in cloud complexes that are all very similar.

V. CLOUD BLENDING

Four of the H I emission features in Figure 1, at $(l, v) = (24, 102)$, (30.5, 94), (50.5, 53) and (55.5, 38), are located at the tangent points to spiral arms (cf. § VII). These features are almost certainly blends of several independent H I clouds along the lines of sight, especially since the features at (24, 102N), (50.5, 53) and (55.5, 38) are associated with three, four, and two independent CO clouds spanning distances of 3.1 kpc, 3.9 kpc, and 2.6 kpc, respectively. Five of the H I features, at (19.5, 42), (23, 54), (24, 102), (31, 47) and (31.5, 13), probably contain contributions from both near and far kinematic distances, because both near and far CO clouds are within the same (l, b, v) coordinate intervals. The masses of these H I clouds have been estimated accordingly, as discussed in § II*d*. For these five clouds, and for the four clouds tangent to the spiral arms, the velocity spread of the H I emission should not be representative of internal turbulence.

Most of the other H I clouds contain only one CO feature, or a cluster of CO features, all at approximately the same distance. In the case of a cluster, the distance range of the CO clouds associated with an H I feature is comparable to the transverse dimension of the feature, so most of the complexes appear to be somewhat round, or localized, in the galactic plane. This is the case for CO clouds in the H I features (12, 14), (13.5, 47), (15, 28), (19.5, 42N), (23, 54N), (31.5, 13N), (39.5, 33), and (47.5, 57). These clusters may be examples of hierarchical structures in the interstellar medium.

VI. TURBULENCE, ROTATION, AND GRAVITATIONAL SELF-BINDING

The 25 H I features in Table 1 that are neither near-far distance blends, nor at the spiral arm tangent points, appear to have 21 cm line widths that result from internal turbulence or orbital motions of clumps inside discrete cloud complexes, with a possible contribution from background Galactic rotation and shear. These line widths are now compared to the expected shear velocities calculated from the Galactic rotation curve, and to the virial theorem velocity dispersions calculated from the derived masses and radii. The critical densities for self-gravitational binding in the tidal force field of the Galaxy are also compared to the observed densities.

The total mass of a complex, M, is taken from column (4) in Table 4. The radius, R, is defined by the equation

$$R = \frac{D}{\pi}\,[(l_{\max} - l_{\min})(b_{\max} - b_{\min})]^{1/2}, \tag{10}$$

where the longitude and latitude ranges are from Table 1, converted into radians. This radius is only approximate because the H I cloud boundaries are imprecise. The line width is also approximate, taken from the velocity range in Table 1,

$$\Delta v_{\text{total}} = v_{\max} - v_{\min} \,. \tag{11}$$

This line width usually extends for as far as the H I feature can be seen in the contours of Figure 1*a*. This extent is typically about five temperature contour levels for the brightest clouds, so many of the line widths are measured at essentially one-fifth of the peak temperature. For a Gaussian line profile, the dispersion, σ, that corresponds to a full line width Δv_{total} measured out to a fraction $1/F$ of the peak temperature is given by the equation

$$\sigma = \Delta v_{\text{total}}(8 \ln F)^{-1/2}. \tag{12}$$

Cloud radii, F values, and velocity dispersions calculated from equation (12) are given in Table 5 for the unblended H I complexes. Average cloud densities obtained from the equation

$$n = \frac{3M}{4\pi R^3 \mu} \tag{13}$$

are also given, as are the turbulent pressures normalized to the Boltzmann constant, k_B,

$$P_{\text{turb}} = n\mu\sigma^2/k_B \,. \tag{14}$$

The turbulent pressure often exceeds the average interstellar pressure around the Sun by a factor of 10 or more.

A possible contribution to the velocity dispersion resulting from background Galactic shear may be estimated from the rotation curve given by Schmidt (1965). The angular velocity around the Galactic center is $\Omega(r)$, for galactocentric distance, r. The expected radial velocity for a cloud at longitude l and distance D from the Sun is $v_{\text{rad}} = R_\odot(\Omega[r] - \Omega_\odot)\sin(l)$, where $r^2 = 100 + D^2 - 20D\cos(l)$. The mean squared relative radial velocity, Δv_s, of points inside a shearing circular region having a radius and position equal to the radius and position of a giant H I cloud is evaluated from the equation

$$\Delta v_S{}^2 = \frac{\int_0^R \int_0^{2\pi} (v_{\text{rad}}[s, \theta] - v_{\text{rad},0})^2 d\theta s ds}{\int_0^R \int_0^{2\pi} d\theta s ds}, \tag{15}$$

where $v_{\text{rad},0}$ is the radial velocity of the cloud center, s and θ are radial and angular coordinates inside the shearing circle, and R is the cloud's radius (Table 5). The ratio $\Delta v_s/\sigma$ is a measure of the possible importance of shear. These ratios are in Table 5 for the unblended clouds. The ratios are moderately large (the average is 0.40 ± 0.22), so shear could be an important contribution to the linewidth if the clouds are unbound.

For bound clouds, in which the density is large enough for

TABLE 5

CHECKS ON SELF-GRAVITATIONAL BINDING

(l, v) (°, km s^{-1})	Radius (pc)	F	σ (km s^{-1})	n (cm^{-3})	P_{turb}/k_B ($\times 10^3$ cm^{-3} K)	v_{VT} (km s^{-1})	$\Delta v_s/\sigma$	n/n_{crit}	v_{VT}/σ
10.5, 33	113	5	4.7	11.9	42	4.7	0.44	2.8	1.00
12, 6..............	53	5	1.1	3.7	0.74	1.2	0.65	1.4	1.11
12, 14	161	5	5.6	16.4	81	7.9	0.40	5.1	1.41
13.5, 32	119	3	5.1	14.4	59	5.5	0.40	3.5	1.08
13.5, 47	146	4	4.5	13.9	45	6.6	0.57	3.0	1.46
15, 28	150	5	4.2	11.4	32	6.1	0.58	2.8	1.47
26, 105	140	4	8.1	10.8	114	5.6	0.06	2.2	0.69
27, 64	97	4	6.0	10.4	60	3.8	0.15	2.6	0.63
30, 78	217	5	7.0	7.7	59	7.3	0.21	1.9	1.05
34, 50	108	5	7.5	19.9	180	5.8	0.12	5.9	0.77
34, 95	116	3	7.1	14.8	118	5.4	0.10	3.5	0.76
36, 58	304	3	5.1	4.3	18	7.7	0.61	1.2	1.51
37.5, 81	362	3	6.1	3.4	20	8.0	0.55	0.87	1.33
39.5, 33	249	6	6.6	2.7	19	4.9	0.29	0.85	0.75
40, 64	420	3	8.1	3.3	35	9.3	0.55	0.93	1.14
41, 62	285	3	5.4	7.6	35	9.5	0.58	2.2	1.76
46, 28	118	4	5.7	4.2	22	2.9	0.17	1.4	0.51
47.5, 57	430	6	5.8	4.0	21	10.3	0.87	1.2	1.78
48.5, 20	236	2	3.4	7.3	13	7.7	0.85	2.6	2.27
52, 24	84	2	5.1	7.1	30	2.7	0.15	2.5	0.53
57.5, 35	109	3	5.4	10.7	50	4.3	0.25	3.5	0.80
58, 18	106	4	4.2	4.9	14	2.8	0.27	1.8	0.68
62.5, 26	135	4	4.5	5.3	17	3.8	0.38	1.8	0.83
64.5, 20	88	2	4.2	7.5	21	2.9	0.27	2.7	0.68
70, 11	86	5	2.8	7.1	8.8	2.8	0.41	2.7	1.00

gravitational binding to offset the background Galactic tidal force, there may be no internal shear because the cloud is detached from the background Galactic flow. Then the derived ratio $\Delta v_s/\sigma$ is inapplicable. In fact, the average densities for the many of the cloud complexes (Table 5) appear to be large enough to permit self-gravitational binding in the tidal force field of the Galaxy. The tidal acceleration per unit length is given by the quantity

$$T = -2\Omega r \frac{d\Omega}{dr} . \tag{16}$$

For self-gravitational binding of a cloud that is corotating around the Galaxy, i.e., with no additional spin in the rotating frame, the cloud radius and mass must satisfy the equation $GM/R^3 > T$, which may be written as a lower limit to the average cloud density,

$$n > n_{crit} = \frac{3T}{4\pi G\mu} . \tag{17}$$

Equation (17) is the same as equation (14-21) in Mihalas and Routly (1968), which is for the similar problem of tidal disruption of a star cluster. The assumed lack of spin in the rotating frame is in agreement with observations, as discussed below.

Table 5 gives the ratio of the observed densities to the critical densities. These ratios are usually comparable to or larger than 1 (the average value is 2.4 ± 1.2), in which case the clouds could be bound. Of course, the observed densities are inaccurate, as are the critical densities for tidal binding. The critical density may vary with phase in a spiral density wave, taking lower than average values in the spiral arms where the rotation curve becomes more like a solid body (Elmegreen 1987*b*; see Rubin, Ford, and Thonnard 1980, and especially the rotation curve for NGC 2998). Some of the lower density complexes, or perhaps all of the complexes, may be bound only while they are in the spiral arms; they may come apart when they enter an interarm region.

Another way to assess the degree of self-gravitational binding is to compare the one-dimensional virial theorem velocity dispersion, v_{VT}, to the observed H I velocity dispersions, σ. The virial dispersion is derived from the equation

$$v_{VT}{}^2 = \frac{GM}{2R(1+\beta)} , \tag{18}$$

which applies to a spherical cloud with an isothermal density profile (density varies as the inverse square of the distance from the center), an external pressure, and a magnetic field pressure equal to the factor β times the turbulent pressure (see Appendix A in Elmegreen and Clemens 1985). The M in equation (18) is taken equal to the total mass of the complex, from column (4) in Table 4, and the radius is from equation (10), given in Table 5, β was arbitrarily taken equal to 1 because magnetism is likely to contribute to cloud support. The derived ratios v_{VT}/σ are in Table 5. Evidently the ratios are close to 1, indicating again that self-gravity may bind some of the clouds.

Figure 5 shows the line width ratio versus the total cloud mass for the unblended clouds with cataloged CO emission. A slight correlation with mass suggests that other contributions to the line width could be present for small clouds (more turbulence and less magnetism, for example), or that large clouds are less centrally condensed than small clouds (which could decrease the velocity ratio for large clouds by the factor $0.6^{0.5} = 0.77$), or that the procedure for determining the masses, radii, and line widths contain slight systematic errors. Because the definition of a cloud complex is somewhat arbitrary, as are the spatial and velocity extents of each cloud, and because the H I and H_2 masses, mass distributions and magnetic field strengths are uncertain, the derived ratio of $v_{VT}/\sigma \approx 0.5$–2 is suggestive, but not conclusive, that the clouds are gravitationally bound.

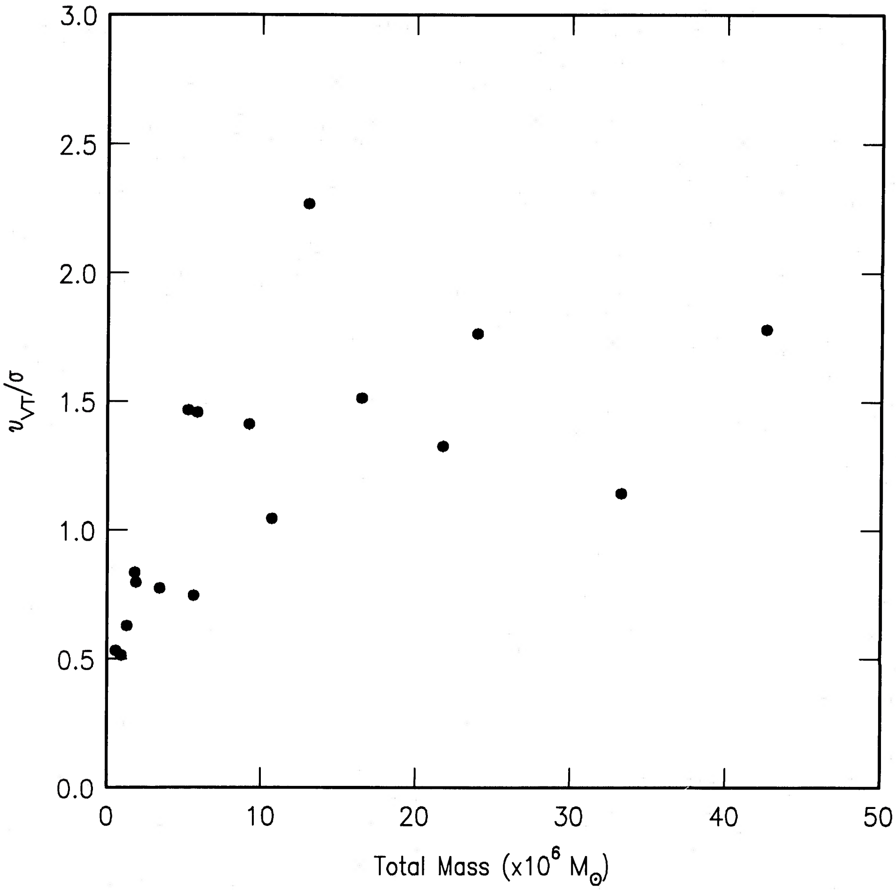

FIG. 5.—The ratio of the one-dimensional virial-theorem velocity dispersion to the observed 21 cm velocity dispersion is plotted against the total cloud mass

The tidal stability criterion derived by Stark and Blitz (1978) also gives no conclusive result for these clouds. Blitz and Glassgold (1982) wrote this criterion in terms of the quantities $x = (GM/TR^3)^{1/3}$ and $a = 0.5(v^2/TR^2 - 1)$, in which case the condition for binding is

$$x^3 - 1.5x^2 - a > 0 . \quad (19)$$

In our notation, $x^3 = n/n_{\rm crit}$ and $v^2/TR^2 = (n/n_{\rm crit})(2v_{\rm VT}/\sigma)^{-2}$, so the condition is

$$\frac{n}{n_{\rm crit}}\left(1 - \frac{1}{8(v_{\rm VT}/\sigma)^2}\right) - 1.5\left(\frac{n}{n_{\rm crit}}\right)^{2/3} + 0.5 > 0 . \quad (20)$$

This quantity was evaluated for the unblended clouds. The result scattered around zero, with an average of approximately -0.11 ± 0.33. A problem with the use of this method is that the required parameters are difficult to measure. The cloud radius that appears in the equation is the distance between the cloud center and the cloud edge in the direction of the galactic center, which is not generally the same as the radius in equation (10); the velocity dispersion that appears is the value near the cloud edge, not the rms value for the whole cloud. The resultant criterion is relatively insensitive to the velocity ratio once $v_{\rm VT}/\sigma$ exceeds ~ 2; it is more sensitive to the density ratio. For example, as the ratio of the virial velocity to the observed dispersion increases from 1 to 2 to ∞, the minimum ratio between the observed density and the critical density decreases from 3.0 to 1.6 to 1. Neither the derived densities nor the critical densities are known to within a factor of 2, so the criterion cannot determine the state of gravitational binding any better than the other tests here. Nevertheless, criterion (20) suggests that the clouds are not grossly unbound, and that many of them could be bound, especially if they are elongated in the azimuthal direction (and the R implicit in eq. [20] is less than the R in eq. [10]). Such azimuthal elongation may be appropriate. The Sagittarius-arm CO complexes studied by Dame *et al.* (1986; see their Fig. 10) show azimuthal orientations because the CO boundaries are ellipsoidal at small Galactic longitudes, where azimuthally oriented clouds would be viewed broadside, and they are circular at large longitudes, near the spiral arm tangent direction, where azimuthally oriented clouds would be viewed end on. The M16/M17 H I cloud at $(l, v) = (12, 14)$ is an example because it is clearly elongated in Figure 2. The value of the left-hand side of criterion (20) for this cloud is 0.82, which places it in the bound regime.

The rotation of cloud complexes is also difficult to determine from the data. The H I complex surrounding M16 and M17, which is denoted by $(l, v) = (12, 14)$, appears to be rotating from our perspective because the centroid velocity varies systematically with longitude (see Fig. 1). This velocity shift is parallel to the curve that traces the Sagittarius spiral arm on an (l, v) diagram (i.e., the ellipsoidal outline of the H I cloud points toward the adjacent clouds on the Sagittarius arm; see § VII*b*), so in fact there is no noticeable velocity shift or rotation in the cloud's local standard of rest. The apparent velocity shift on an (l, v) diagram is the result of the H I cloud and the solar neighborhood having different angular velocities around the Galactic center; i.e., the M16/M17 H I cloud could be corotating around the center. Other H I clouds could be corotating also, but their angular extents are too small to make this corotation noticeable. Corotation of the M17 cloud implies that the gas lost angular momentum as it condensed from the ambient interstellar medium.

VII. IMPLICATIONS

a) Fractional Luminosity, Mass, Volume, and Kinetic Energy in the Form of Giant Cloud Complexes

A large fraction of the H I emission from the first Galactic quadrant appears to originate in the 38 cataloged cloud complexes. The clipping procedure used here ($T_A > 40$ K) isolates 60% of all the emission (§ II), and of this brightest emission, 74% is in the complexes listed in Table 1. Thus $0.6 \times 0.74 = 0.44$ of all the H I emission from the first quadrant is in the bright cataloged complexes. Of the unclipped emission, 68% is within the boundaries of the complexes, i.e., is within the (Δl, Δv) coordinate intervals that define the complexes. Because most of these emission regions appear to be discrete clouds or cloud complexes, some of which may be gravitationally bound, a fraction between 40% and 70% of all of the H I emission from the first Galactic quadrant appears to be associated with, or inside, one or another giant H I cloud. A minimum fraction may be obtained for the 25 unblended clouds discussed in §§ V and VI, whose summed, temperature-clipped emission represents 35% of the total unclipped 21 cm emission from the first quadrant.

The mass fraction in complexes is larger than the emission fraction if the complexes are clumpy and optically thick. The estimated H I mass for all of the complexes is $2.38 \times 10^8\ M_\odot$, obtained from the sum of the masses in column (5) of Table 2. These masses are derived in § III*b* under the assumption that each temperature-clipped complex is composed of unresolved clumps with a spin temperature of 120 K, separated by a 1000 K interclump medium representing one-third of the total complex mass; each unresolved clump was also assumed to have a velocity dispersion of 4 km s^{-1} and an optical depth of 1. These parameters are consistent with the H I absorption-line clumps that are observed on the lines of sight through the complexes (Table 3). Because the sum of the *optically thin*, temperature-clipped masses (col. [1] in Table 2) is 1.04×10^8 $M_\odot$, the total H I mass in complexes increases by a factor of 2.3 as a result of the assumed opacity and clumpiness. If the H I emission that comes from outside the cataloged complexes and from the low-temperature lines of sight ($T_A < 40$ K) is optically thin, then this remaining fraction, $1 - 0.44 = 0.56$, of the emission, multiplied by some effective distance squared, is directly proportional to the H I mass (i.e., no opacity corrections necessary). If, in addition, the fraction of the mass in complexes is independent of distance, then the effective distance for conversion from emission to mass on each line of sight is the same for the low-intensity emission as it is for the bright complexes. In that case, the total mass of all of the H I is increased by the assumed opacity and clumpiness by a factor $0.56 + 0.44 \times 2.3 = 1.57$. This implies that the mass of H I in the first Galactic quadrant is larger than previously thought (under the assumption of low optical depths) by approximately 60%. This is consistent with the estimated mass correction for opacity made by Dickey and Benson (1982). This result also implies that the mass fraction in the cataloged complexes is $2.3 \times 0.44/1.57 = 0.64$, which is larger than the luminosity fraction of 0.44 discussed above. This mass fraction might be a lower limit because some of the clumps inside each complex could be cooler than the assumed 120 K.

The excess mass resulting from clumpiness alone can be determined by comparing columns (4) and (5) in Table 2, because column (4) is for uniform, optically thick emission ($T_s = 120$ K) and column (5) is for clumpy, optically thick emission ($T_c = 120$ K). The total mass from column (4) is $2.07 \times 10^8\ M_\odot$, which is 2.0 times the total complex mass for optically thin emission (col. [1]). If the low-brightness lines of sight are also optically thin, then the total H I mass for uniform complexes at $T_s = 120$ K is larger than the total mass for optically thin complexes by the factor $0.56 + 0.44 \times 2.0 = 1.44$. The assumed clumpiness therefore contributes an extra factor of $1.57/1.44 = 1.09$ to the H I mass.

Although the cataloged cloud complexes may contain $\sim 64\%$ of the H I mass in the first quadrant, they occupy only a small fraction of the total volume. The total volume of all of the unblended clouds in Table 5 is 1.34×10^9 pc^3 ($= \sum 4\pi R^3/3$). The blended clouds contribute an additional 40% to the mass, so if they contribute a similar fraction to the volume then the total volume of the complexes equals approximately 1.9×10^9 pc^3. The volume of the first quadrant equals 4.7×10^{10} pc^3 for a galactocentric distance of 10 kpc and a disk thickness of 300 pc. Thus the clouds occupy $\sim 4\%$ of the volume of interstellar matter. (This fraction should not be confused with the filling factor of individual diffuse clouds in the solar neighborhood.) Within the spiral arms the filling factor of the complexes is much higher than 4%. If, for example, the spiral arms occupy $\sim 25\%$ of the volume of the Galactic disk, then the clouds occupy $\sim 16\%$ of the volume of the arms. This 16% is consistent with the ratio of the size of a complex (~ 200 pc) to their separation (~ 1500 pc) along an arm, which is another measure of the volume filling factor because the clouds are nearly aligned in a linear string along the arms (see Fig. 9 in Dame *et al.* 1986). If $\sim 64\%$ of the H I mass is in $\sim 16\%$ of the volume of the spiral arms, then the average density enhancement in each cloud is a factor of ~ 4 above the average ambient density. This density enhancement is consistent with the cloud densities given in Table 5, which, for the unblended clouds, have an average value of 8.8 ± 4.7 cm^{-3}.

Because the mass fraction for cloud complexes is so large, and because some or all of the clouds could be gravitationally bound (§ VI), the kinetic energy from virialized motions may be a significant fraction of the random kinetic energy of the interstellar gas. Suppose that 64% of the H I mass in the first quadrant has the average one-dimensional velocity dispersion listed in Table 5, which is ~ 5.3 km s^{-1}. This velocity dispersion is comparable to the one-dimensional cloud-to-cloud dispersion for local diffuse clouds, so a fraction equal to the complex mass fraction, $\sim 64\%$, of the interstellar random kinetic energy could be virialized motions in cloud complexes. Not all of this kinetic energy is gravitational in origin. If a 10^7 $M_\odot$ piece of interstellar matter condenses from the average interstellar density to a density ~ 4 times larger (and therefore looks like one of the cloud complexes studied here), and the radius of this piece shrinks by a factor $4^{1/3} = 1.6$, then the gravitational binding energy released from the complex equals $1 - (1/1.6) = 0.38$ of the initial gravitational energy. According to the virial theorem, one-half of this binding energy is radiated away, and the other half goes into the kinetic energy of internal motions. Thus $\sim 19\%$ of the initial binding energy of $\sim 64\%$ of the mass, or $\sim 12\%$ of the gravitational binding energy of the interstellar medium, may continuously cycle through turbulent motions in giant cloud complexes, over time scales equal to the energy dissipation time. In a steady state, this same 12% equals the fraction of the kinetic energy of the interstellar medium that comes from self-gravitational binding in complexes. The other 88% of the kinetic energy is presumably from supernovae, stellar winds, and other sources.

b) Giant Cloud Complexes as Tracers of Galactic Spiral Structure

The brightest CO emission regions trace out at least two spiral arms in the first Galactic quadrant (Dame *et al.* 1986). These arms also show up clearly in bright H I because the temperature-clipped H I (l, v) diagram in Figure 1 is very similar to the temperature-clipped CO (l, v) diagram in Dame *et al.* (1986).

The Sagittarius spiral arm appears in Figure 1, following a sequence of increasing distance, starting with $(l, v) = (12, 14)$, and continuing onto a cluster of clouds containing (31, 47N), (39.5, 33), and (34, 50), and then to the spiral arm tangent point at (50.5, 53), with a possible spur at (55.5, 38), and onto an arc of clouds at (47.5, 57), (41, 62), (40, 64), (36, 58), and (31, 47F). This sequence is also evident in CO (see Table 4 here, and Fig. 10 in Dame *et al.* 1986). Among all of these Sagittarius arm features, only two are clear blends that result from velocity crowding at the spiral arm tangent (50.5, 53) or a near-far distance ambiguity (31, 47). The distance ambiguity occurs because the arm apparently intersects itself, or intersects a spur or local feature, on the (l, v) diagram.

The Norma-Scutum arm appears to extend along a sequence beginning with a cluster of clouds at (10.5, 33), (13.5, 32), and (15, 28), and continuing onto another cluster including (19.5, 42) and (23, 54), and onto the clouds (27, 64) and (30, 78) until the spiral arm tangent occurs at (30.5, 94), with a possible weak spur at (34, 95); then the arm continues back down (in longitude) on the far side of the tangent point, including (26, 105), (24, 102F), and possibly (23, 54F). Only the clouds (24, 102) and (23, 54) are obviously confused by near-far distance ambiguities, and again these clouds occur where the spiral arms intersect each other on the (l, v) diagram. A next inner arm, or piece of arm, seems to include the clouds at (13.5, 47) and (24, 102N), but there is little definition of this arm in either bright H I or CO emission.

Figure 1 indicates that the arm/interarm contrast factor for clipped H I emission is large, perhaps comparable to the contrast in CO (Cohen *et al.* 1980). The interarm gaps are just as clear on Figure 1 as they are in CO (l, v) diagrams. Thus the bright H I emission is a good tracer of Galactic spiral structure. The arm/interarm contrast is much less for the total H I emission, of course, because the low brightness H I shows much less correlation with the spiral arms than the bright H I.

c) Giant Cloud Complexes as the Fundamental Unit for Star Formation in Galaxies

Most of the molecular mass in our Galaxy is in the largest CO complexes (Solomon and Sanders 1980), and most of the atomic mass is in the largest H I complexes (§ III*e*). Because star formation occurs in the cores of these giant cloud complexes, most star formation in our Galaxy is associated with atomic/molecular clouds containing 10^6–10^7 $M_\odot$. The same appears to be true in other galaxies (see references in § I), but not necessarily in all galaxies. This implies that for galaxies like ours, $\sim 10^7$ $M_\odot$ is a fundamental, or largest, scale for star formation. Clouds of this size have been termed "superclouds" to distinguish them from purely molecular "giant" clouds, and to emphasize their important role in the distribution of interstellar mass and star formation.

Superclouds may form by gravitational instabilities in the ambient interstellar gas. According to a recent calculation (Elmegreen 1987*b*), this instability should occur regardless of Galactic rotation and shear, and it should be able to form H I cloud complexes with the observed densities and masses. The formation may be enhanced in density wave spiral arms because the density and magnetic field strength are larger there, and because the large-scale rate of shear is smaller there. Molecular clouds inside the H I clouds may be cooled fragments that condensed out of the atomic gas by additional gravitational instabilities, or they may have formed differently, by the agglomeration of smaller clouds, for example. A problem with the first of these molecular cloud formation mechanisms is that superclouds apparently have too high a velocity dispersion to allow gravitationally driven condensation into individual molecular clouds. The agglomeration model for molecular clouds is not unrealistic, especially if magnetically enhanced collision cross sections are considered (see references in Elmegreen 1987*c*). Agglomeration may occur either during the growth of the primary instability that forms the supercloud, or it may occur at a different time. Giant molecular clouds inside superclouds also could have formed elsewhere and simply been brought together by the same forces that collected the atomic gas.

The presence of superclouds in galactic spiral arms seems to imply that the conditions for forming superclouds are more favorable in the arms, and it may also imply that a supercloud is disassembled as it flows into the interarm region. A possible cloud destruction mechanism is the Galactic tidal force, which is larger in the interarm regions than in the arms (Elmegreen 1987*b*). Superclouds could form in the arms by gravitational instabilities, and then get torn apart by increased tidal forces in the interarm regions. The molecular clouds may not get torn apart by the increased tidal forces, however, because their density is too high. Interarm regions might therefore contain bare molecular clouds, unlike the arm regions.

d) On the Origin of the Molecular Ring in the Galaxy

The decrease in the average molecular fraction of interstellar matter with increasing galactocentric distance, combined with the general deficiency of gas in the region of the Galactic bulge, gives the molecular distribution in our Galaxy the appearance of a ring, centered at ~ 5–6 kpc (Scoville and Solomon 1975; Gordon and Burton 1976). Because this decrease is strongly reflected in the molecular fractions of individual superclouds (§ IV), and because these clouds dominate the total gas mass in the Galaxy (§ VII*a*), the average molecular fraction of the gas appears to be decreasing with distance because the mass or number of molecular cores inside each supercloud decreases. The mass in each supercloud is relatively independent of galactocentric distance.

The variation in the molecular fraction per cloud may be the result of a variation in the average pressure and radiation field in the exponential-like disk of our Galaxy. Clouds in the inner Galaxy probably have larger pressures, and, therefore, larger densities and column densities for a given mass, than clouds in the outer Galaxy. Molecular-line shielding of background UV radiation should therefore be more important for the inner

Galaxy clouds, so these clouds should have higher molecular fractions.

The molecular fraction, η, of an ensemble of diffuse clouds, having a mass distribution function $f(M)dM \propto M^{-\alpha}dM$ with $\alpha \approx 4/3$ (Knude 1979) varies with the UV radiation field ϕ and the pressure P as (Stark, Elmegreen, and Chance 1987)

$$\eta(\phi, P) = 1 - (1 - \eta_0)\left(\frac{\phi}{\phi_0}\right)^2\left(\frac{P_0}{P}\right)^{10/3\gamma}, \tag{21}$$

where η_0, ϕ_0, and P_0 are fiducial values used for scaling, and γ is the adiabatic index, defined such that $P \propto \rho^\gamma$ for density ρ. Molecule formation in clouds has been assumed to require that a self-shielding layer exists; this criterion corresponds to a minimum value of the product of the density and the column density. If the radiation field and the pressure vary with galactocentric distance r in the same way, i.e., $\phi \propto P$, and if $\gamma = \frac{2}{3}$ from Jura (1976), then for two different radii r_1 and r_2,

$$\eta(r_2) = 1 - (1 - \eta[r_1])\left(\frac{P[r_1]}{P[r_2]}\right)^3, \tag{22}$$

with the constraint that $0 < \eta < 1$. Suppose r_1 represents the solar neighborhood with $\eta_1 \approx 0.1$, as discussed in § IV. If the pressure and radiation field are larger in the molecular ring (r_2) by a factor of 1.5, then the average molecular fraction there would be 0.73, which is similar to that observed (cf. Fig. 4). The systematic variation in the molecular fraction per supercloud, and the corresponding variation in the average molecular fraction of interstellar gas, could therefore be partially the result of small and systematic pressure variations throughout the galactic disk.

The tape version of the Weaver-Williams survey was kindly prepared for us in (l, b, v, T) format by Dr. E. Gottlieb. We thank Vassar College undergraduates Nicola Lemmen and Derek Wallentinsen for their preliminary determination of the mass of cloud (l, v) = (12, 14). We are also grateful to the Institute for Theoretical Physics in Santa Barbara, California, for their hospitality during the initial phases in this research. Research there was supported by the National Science Foundation, grant PHY82-17853, with supplementary funding from NASA. D. M. E. was supported in part by the National Science Foundation Visiting Professorship for Women program. Helpful comments by Dr. S. M. Fall, regarding shear, and by the referee, Dr. C. Heiles, are gratefully appreciated.

APPENDIX

RADIATIVE TRANSFER FOR A CLUMPY CLOUD

The intensity of radiation from a region composed of unresolved clumps and an interclump medium at a different excitation temperature is derived here. The clumps are assumed to be identical, with excitation temperature T_c and opacity τ_c. The interclump medium is assumed to have a uniform excitation temperature, T_i, and a total opacity on the line of sight, τ. The *expected* number of clumps that contribute to the emission and absorption of radiation in a particular velocity interval Δv is assumed to equal ϵ, but the *actual* number on any particular line of sight is denoted by N, which is distributed randomly around the value ϵ according to Poisson statistics.

A line of sight is partitioned by the N clumps into $N + 1$ segments of interclump gas, with opacities τ_i for $i = 1 \rightarrow N + 1$. For $N = 1$, the brightness temperature, T, on the line of sight is the sum of the emission from the nearest interclump segment, plus the emission from the clump with absorption from the nearest interclump segment, plus emission from the distant interclump segment, with absorption from both the clump and the nearest interclump segment,

$$\begin{aligned} T_1 &= T_i(1 - e^{-\tau_1}) + T_c(1 - e^{-\tau_c})e^{-\tau_1} + T_i(1 - e^{-\tau_2})e^{-\tau_1-\tau_c} \\ &= T_i(1 - e^{-\tau-\tau_c}) - (T_i - T_c)(1 - e^{-\tau_c})e^{-\tau_1}, \end{aligned} \tag{A1}$$

where $\tau \equiv \tau_1 + \tau_2$.

For $N = 2$, the brightness temperature is determined in a similar fashion,

$$\begin{aligned} T_2 &= T_i[(1 - e^{-\tau_1}) + (1 - e^{-\tau_2})e^{-\tau_1-\tau_c} + (1 - e^{-\tau_3})e^{-\tau_1-\tau_2-2\tau_c}] + T_c(1 - e^{-\tau_c})(e^{-\tau_1} + e^{-\tau_1-\tau_2-\tau_c}) \\ &= T_i(1 - e^{-\tau-2\tau_c}) - (T_i - T_c)(1 - e^{-\tau_c})(e^{-\tau_1} + e^{-\tau_1-\tau_2-\tau_c}), \end{aligned} \tag{A2}$$

where $\tau = \tau_1 + \tau_2 + \tau_3$.

The notation is simplified by defining the quantities

$$A_N = T_i(1 - e^{-\tau-N\tau_c}) \tag{A3}$$

$$B = (T_i - T_c)(1 - e^{-\tau_c}). \tag{A4}$$

Then the brightness temperature for arbitrary N is

$$T_N = A_N - B\sum_{i=1}^{N} e^{-\sum_{j=1}^{i}\tau_j - (i-1)\tau_c} \tag{A5}$$

This brightness temperature must be averaged over all possible positions of the clumps on a line of sight, weighted according to the probability of each combination of positions. The positions are determined by the variables τ_i. Given the positions of the $N - 1$

nearest clouds, the most distant cloud on the line of sight can have its adjacent interclump opacity, τ_N, range with equal probability anywhere between 0 and $\tau - \sum_{i=1}^{N-1} \tau_i$. The average contribution to the total brightness temperature from this most distant cloud is therefore

$$\frac{1}{\tau - \sum_{i=1}^{N-1} \tau_i} \int_0^{\tau - \sum_{i=1}^{N-1} \tau_i} T_N \, d\tau_N \,. \tag{A6}$$

The next most distant cloud can have its adjacent interclump opacity, τ_{N-1}, range anywhere between 0 and $\tau - \sum_{i=1}^{N-2} \tau_i$, but the probability that the interclump opacity is between τ_{N-1} and $\tau_{N-1} + d\tau_{N-1}$ *and* that the Nth cloud is beyond the $N-1$ cloud, is $(\tau - \sum_{i=1}^{N-1} \tau_i) d\tau_{N-1} / (\tau - \sum_{i=1}^{N-2} \tau_i)^2$. The contribution to the brightness temperature from the two most distant clouds is therefore

$$\left(\tau - \sum_{i=1}^{N-2} \tau_i\right)^{-2} \int_0^{\tau - \sum_{i=1}^{N-2} \tau_i} \int_0^{\tau - \sum_{i=1}^{N-1} \tau_i} T_N \, d\tau_N \, d\tau_{N-1} \,. \tag{A7}$$

In general, the probability of each value of τ_j is the probability that the jth cloud is separated from the $j-1$ cloud by the opacity τ_j and that all of the remaining $N-j$ clouds are beyond the jth cloud. This probability equals

$$\frac{(\tau - \sum_{i=1}^{j} \tau_i)^{N-j} d\tau_j}{(\tau - \sum_{i=1}^{j-1} \tau_i)^{N-j+1}} \,. \tag{A8}$$

The average brightness temperature from N clouds is therefore

$$\begin{aligned} \langle T_N \rangle &= \frac{N!}{\tau^N} \int_0^{\tau} \int_0^{\tau-\tau_1} \int_0^{\tau-\tau_1-\tau_2} \cdots \int_0^{\tau - \sum_{i=1}^{N-2} \tau_i} T_N \, d\tau_N \cdots d\tau_3 \, d\tau_2 \, d\tau_1 \,. \\ &= T_i(1 - e^{-\tau}) e^{-N\tau_c} + T_c(1 - e^{-N\tau_c}) \end{aligned} \tag{A9}$$

The factor of $N!$ is because the clouds can occur in any order (i.e., there are $N!$ permutations of the N clouds).

Now the average temperature for N clouds must be integrated over all possible numbers of clouds, weighted according to the Poisson probability distribution function for mean cloud number ϵ:

$$\begin{aligned} \langle T \rangle &= \sum_{N=0}^{\infty} e^{-\epsilon} \frac{\epsilon^N}{N!} \langle T_N \rangle \\ &= T_i(1 - e^{-\tau}) \exp\left[-\epsilon(1 - e^{-\tau_c})\right] + T_c\{1 - \exp\left[-\epsilon(1 - e^{-\tau_c})\right]\} \end{aligned} \tag{A10}$$

This last expression comes from combining ϵ^N in equation (A10) and $e^{-N\tau_c}$ in equation (A9) to give $(\epsilon e^{-\tau_c})^N$, and the sum of this quantity divided by $N!$ equals $\exp(\epsilon e^{-\tau_c})$. Equation (A10) gives the expected brightness temperature for a randomly clumped line of sight through a cloud complex.

APPENDIX B

A SIMPLE MODEL OF EMISSION FROM A CLUMPY CLOUD

The masses of clumpy clouds that have brightness temperatures that vary with a Gaussian distribution in projected radius R, and velocity, v, are calculated here for various clump and interclump properties. This illustrates the sensitivity of the clumpy cloud masses to the input parameters. (This model was not used to calculate real cloud masses in the text.)

The brightness temperature in a model cloud is assumed to vary as

$$T_B(R, v) = T_0 \, e^{-0.5(R^2 + v^2)} \,,$$

out to 5 standard deviations in radius and velocity. The clump temperature is taken to be $T_c = 100$ K, the interclump medium temperature is taken to be $T_i = 10^2$ K, 10^3 K, or 10^4 K, and the interclump-to-clump mass ratio is assumed to equal $I = 0.1$, 0.5, and 2. The clump line width does not enter into the final result for this discussion. The clump opacity was allowed to vary between 0 and 4. The cloud center temperature is taken to be 40 K or 80 K.

A cloud mass was derived for each combination of parameters using the clumpy cloud model discussed in § III*b* and Appendix A. The mass was then divided by the optically thin mass, as calculated in § III*a* with $T_s = \infty$. The resultant ratio is plotted in Figure 6 as a function of the clump opacity. This ratio may be viewed as a correction factor for the mass of a clumpy cloud. It ranges between 1 and 2 for typical parameters.

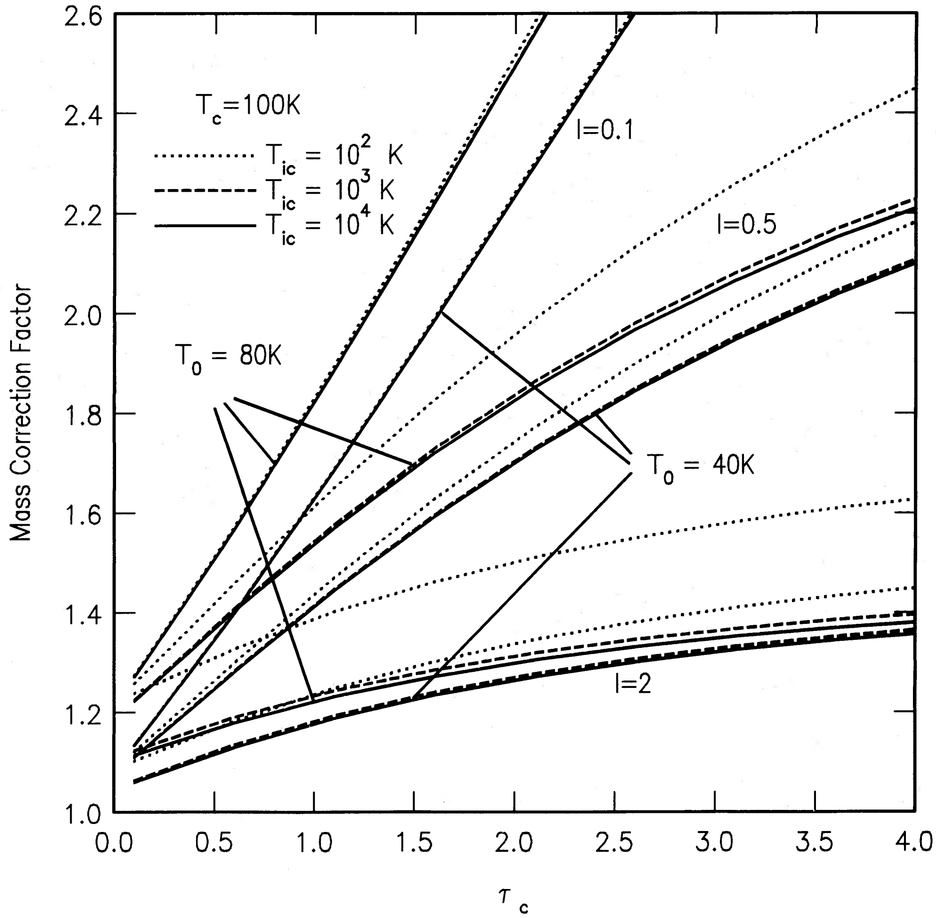

FIG. 6.—The ratio of the clumpy cloud mass to the optically thin cloud mass (the "mass correction factor") is shown as a function of the opacity in each clump, τ_c, for a simple model of clumpy clouds (Appendix B). The cloud-center brightness temperature is denoted by T_0, the ratio of the interclump mass to the total clump mass is denoted by I, and the interclump spin temperature is denoted by T_{ic}. Each clump is assumed to have a spin temperature of 100 K.

REFERENCES

Allen, R. J., and Goss, W. M. 1979, *Astr. Ap. Suppl.*, **36**, 135.
Allen, R. J., Goss, W. M., and van Woerden, H. 1973, *Astr. Ap.*, **29**, 447.
Bajaja, E., and Shane, W. W. 1982, *Astr. Ap. Suppl.*, **49**, 745.
Baker, P. L., and Burton, W. B. 1975, *Ap. J.*, **198**, 281.
———. 1979, *Astr. Ap. Suppl.*, **35**, 129.
Bania, T. M. 1983, *A.J.*, **88**, 1222.
Batrla, W., Wilson, T. L., and Rahe, J. 1981, *Astr. Ap.*, **96**, 202.
Blitz, L. 1985, *Ap. J.*, **296**, 481.
Blitz, L., and Glassgold, A. E. 1982, *Ap. J.*, **252**, 481.
Blitz, L., Israel, F. P., Neugebauer, G., Gatley, I., Lee, T. J., and Beattie, D. H. 1981, *Ap. J.*, **249**, 76.
Bok, B. J., Lawrence, R. S., and Menon, T. K. 1955, *Pub. A.S.P.*, **67**, 108.
Boulanger, F., Bystedt, J., Casoli, F., and Combes, F. 1984, *Astr. Ap.*, **140**, L5.
Boulanger, F., Stark, A. A., and Combes, F. 1981, *Astr. Ap.*, **93**, L1.
Burton, W. B., Listz, H. S., and Baker, P. L. 1978, *Ap. J. (Letters)*, **219**, L67.
Chu, K. W. 1975, Ph.D. thesis, California Institute of Technology.
Cleary, M. N., Heiles, C., and Haslam, C. G. T. 1979, *Astr. Ap. Suppl.*, **36**, 95.
Cohen, R. S., Dame, T. M., and Thaddeus, P. 1986, *Ap. J. Suppl.*, **60**, 695.
Cottrell, G. A. 1976, *M.N.R.A.S.*, **177**, 463.
Crovisier, R. 1981, *Astr. Ap.*, **94**, 162.
Crovisier, J., Kazès, I., and Aubry, D. 1978, *Astr. Ap. Suppl.*, **32**, 205.
Dame, T. M. 1983, Ph.D. thesis, Columbia University.
Dame, T. M., Elmegreen, B. G., Cohen, R. S., and Thaddeus, P. 1986, *Ap. J.*, **305**, 892.
Dame, T. M., *et al.* 1987, *Ap. J.*, submitted.
Davies, R. D., and Cummings, E. R. 1975, *M.N.R.A.S.*, **170**, 95.
Dewdney, P. E. 1982, in *Regions of Recent Star Formation*, ed. R. S. Roger and P. E. Dewdney (Dordrecht: Reidel), p. 181.
Dewdney, P. E., and Roger, R. S. 1982, *Ap. J.*, **255**, 564.
Dickel, H. R., Dickel, J. R., and Wilson, W. J. 1982, in *Regions of Recent Star Formation*, ed. R. S. Roger and P. E. Dewdney (Dordrecht: Reidel), p. 175.
Dickey, J. M., and Benson, J. M. 1982, *A.J.*, **87**, 278.
Dickey, J. M., Kulkarni, S. R., van Gorkom, J. H., and Heiles, C. 1983, *Ap. J. Suppl.*, **53**, 591.
Dickey, J. M., Salpeter, E. E., and Terzian, Y. 1979, *Ap. J.*, **228**, 465.
Dickey, J. M., Weisberg, J. M., Rankin, J. M., and Boriakoff, V. 1981, *Astr. Ap.*, **101**, 332.
Elmegreen, B. G. 1979, in *Phases of Interstellar Matter*, ed. J. M. Dickey (Green Bank: NRAO), p. 25.
———. 1985, in *Birth and Infancy of Stars*, ed. R. Lucas, A. Omont, and R. Stora (Amsterdam: Elsevier Science Publishers B.V.), p. 215.
———. 1987*a*, in *IAU Symposium 115, Star Forming Regions*, ed. M. Peimbert and J. Jugaku (Dordrecht: Reidel), p. 457.
———. 1987*b*, *Ap. J.*, **312**, 626.
———. 1987*c*, in *Interstellar Processes*, ed. D. Hollenbach and H. Thronson (Dordrecht: Reidel), in press.
Elmegreen, B. G., and Clemens, C. 1985, *Ap. J.*, **294**, 523.
Emerson, D. T. 1974, *M.N.R.A.S.*, **169**, 607.
Gordon, C. P., Gordon, K. J., and Jacobson, M. R. 1976, *Ap. J.*, **203**, 593.
Gordon, M. A., and Burton, W. B. 1976, *Ap. J.*, **208**, 346.
Gottesman, S. T., and Weliachew, J. 1977, *Astr. Ap.*, **61**, 253.
Grabelsky, D. A. 1985, Ph.D. thesis, Columbia University.
Grabelsky, D. A., Cohen, R. S., May, J., Bronfman, L., and Thaddeus, P. 1987, *Ap. J.*, submitted.
Hasegawa, T., Sato, F., and Fukui, Y. 1983, *A.J.*, **88**, 658.
Henderson, A. P., Jackson, P. D., and Kerr, F. J. 1982, *Ap. J.*, **263**, 116.
Jenkins, E. B. 1970, in *IAU Symposium 36, Ultraviolet Stellar Spectra and Related Ground-based Observations*, ed. L. Houziaux and H. E. Butler (Dordrecht: Reidel), p. 281.
Jura, M. 1976, *A.J.*, **81**, 178.
Knapp, G. R. 1974, *Astr. Ap.*, **79**, 527.
Knude, J. 1979, *Astr. Ap. Suppl.*, **38**, 407.
Kulkarni, S. R., and Heiles, C. 1987, in *Galactic and Extragalactic Radio Astronomy*, ed. K. I. Kellerman and G. L. Verschuur (New York: Springer Verlag), in press.
Lazareff, B. 1975, *Astr. Ap.*, **42**, 25.
Linke, R. A. 1982, in *Extragalactic Molecules*, ed. L. Blitz and M. Kutner (Green Bank: NRAO Publications Office), p. 87.

Liszt, H. S. 1983, *Ap. J.*, **275**, 163.
Liszt, H. S., Burton, W. B., and Bania, T. M. 1981, *Ap. J.*, **246**, 74.
Mattila, K., and Sandell, G. 1979, *Astr. Ap.*, **78**, 264.
McGee, R. X., and Milton, J. A. 1964, *Australian J. Phys.*, **17**, 128.
———. 1966, *Australian J. Phys.*, **19**, 343.
Mebold, U., and Hills, D. L. 1975, *Astr. Ap.*, **42**, 197.
Mebold, U., Winnberg, A., Kalberla, P. M. W., and Goss, W. M. 1982, *Astr. Ap.*, **115**, 223.
Mihalas, D., and Routly, P. M. 1968, in *Galactic Astronomy* (San Francisco: Freeman), p. 239.
Minn, Y. K. 1981, *Astr. Ap.*, **103**, 269.
Myers, P. C., Dame, T. M., Thaddeus, P., Cohen, R. S., Silverberg, R. F., Dwek, E., and Hauser, M. G. 1986, *Ap. J.*, **301**, 398.
Myers, P. C., Ho, P. T. P., Schneps, M. H., Chin, G., Pankonin, V., and Winnberg, A. 1978, *Ap. J.*, **220**, 864.
Nakano, M., Ichikawa, T., Tanaka, Y. D., Nakai, N., and Sofue, Y. 1986, *Pub. Astr. Soc. Japan*, in press.
Newton, K. 1980*a*, *M.N.R.A.S.*, **190**, 689.
———. 1980*b*, *M.N.R.A.S.*, **191**, 615.
Page, T., and Carruthers, G. R. 1981, *Ap. J.*, **248**, 906.
Payne, H. E., Salpeter, E. E., and Terzian, Y. 1983, *Ap. J.*, **272**, 540.
Peters, W. L. III., and Bash, F. N. 1982, in *Regions of Recent Star Formation*, ed. R. S. Roger and P. E. Dewdney (Dordrecht: Reidel), p. 469.
Poppel, W. G. L., Rohlfs, K., and Celnik, W. 1983, *Astr. Ap.*, **126**, 152.
Read, P. L. 1980, *M.N.R.A.S.*, **192**, 11.
———. 1981*a*, *M.N.R.A.S.*, **194**, 863.
———. 1981*b*, *M.N.R.A.S.*, **195**, 371.
Roger, R. S., and Irwin, J. A. 1982, *Ap. J.*, **256**, 127.
Rots, A. H. 1975, *Astr. Ap.*, **45**, 43.
Rubin, V. C., Ford, W. K., Jr., and Thonnard, N. 1980, *Ap. J.*, **238**, 471.
Rydbeck, G., Hjalmarson, Å, Johansson, L. E. B., and Rydbeck, O. E. H. 1986, in *IAU Symposium 115, Star Forming Regions*, ed. M. Peimbert and J. Jugaku (Dordrecht: Reidel), 535.
Saito, T., Ohtani, H., and Tomita, Y. 1981, *Pub. Astr. Soc. Japan*, **33**, 327.
Sancisi, R., Goss, W. M., Anderson, C., Johansson, L. E. B., and Winnberg, A. 1974, *Astr. Ap.*, **35**, 445.
Sandqvist, A., Lindblad, P. O., and Lindroos, K. P. 1976, *Stars and Galaxies from Observational Points of View*, ed. E. K. Kharadze (Tbilisi: Izdatel'stuo "Metsniereba"), p. 520.
Sato, F. 1977, *Pub. Astr. Soc. Japan*, **29**, 75.
Sato, F., and Fukui, Y. 1978, *A.J.*, **83**, 1607.
Scalo, J. M. 1985, in *Protostars and Planets II*, ed. D. C. Black and M. S. Matthews (Tucson: University of Arizona), p. 201.
Schmidt, M. 1965, in *Stars and Stellar Systems*, Vol. **5**, *Galactic Structure*, ed. A. Blaauw and M. Schmidt (Chicago: University of Chicago Press), p. 513.
Scoville, N. Z., and Solomon, P. M. 1975, *Ap. J. (Letters)*, **199**, L105.
Seilestad, G. A., and Wright, M. C. H. 1973, *Ap. J.*, **184**, 343.
Solomon, P. M., and Sanders, D. B. 1980, in *Giant Molecular Clouds in the Galaxy*, ed. P. M. Solomon and M. G. Edmunds (New York: Pergamon), p. 41.
Spitzer, L., Jr. 1978, *Physical Processes in the Interstellar Medium* (New York: Interscience).
———. 1985, *Ap. J. (Letters)*, **290**, L21.
Stal'bovskii, O. I., and Shevchenko, V. S. 1981, *Sov. Astr.—AJ*, **25**, 25.
Stark, A. A. 1985, in *IAU Symposium 106, The Milky Way Galaxy*, ed. H. van Woerden, R. J. Allen, and W. B. Burton (Dordrecht: Reidel), p. 445.
Stark, A. A., and Blitz, L. 1978, *Ap. J. (Letters)*, **225**, L15.
Stark, A. A., Elmegreen, B. G., and Chance, D. 1987, *Ap. J.*, in press.
Strauss, F. M., Pöppel, W. G. L., and Vieira, E. R. 1979, *Astr. Ap.*, **71**, 319.
Unwin, S. C. 1980*a*, *M.N.R.A.S.*, **190**, 551.
———. 1980*b*, *M.N.R.A.S.*, **192**, 243.
van Albada, G. D. 1980, *Astr. Ap.*, **90**, 123.
Viallefond, F., Allen, R. J., and Goss, W. M. 1981, *Astr. Ap.*, **104**, 127.
Viallefond, F., Goss, W. M., and Allen, R. J. 1982, *Astr. Ap.*, **115**, 373.
Weaver, H., and Williams, D. R. W. 1973, *Astr. Ap. Suppl.*, **8**, 1.
Wilson, T. L., and Minn, Y. K. 1977, *Astr. Ap.*, **54**, 933.
Winnberg, A., Grasshoff, M., Goss, W. M., and Sancisi, R. 1980, *Astr. Ap.*, **90**, 176.
Wright, M. C. H., Warner, P. J., and Baldwin, J. E. 1972, *M.N.R.A.S.*, **155**, 337.

B. G. Elmegreen and D. M. Elmegreen: IBM T. J. Watson Research Center, P.O. Box 218, Yorktown Heights, NY 10598